Environmental and Molecular Mutagenesis 54:429–449 (2013)

Research Article

Hyaluronic Acid-Dependent Protection Against UVB-Damaged Human Corneal Cells

Ji-Min Li,[1] Hsiu-Chuan Chou,[2] Ssu-Han Wang,[2] Chieh-Lin Wu,[1] Yi-Wen Chen,[1] Szu-Ting Lin,[2] Yu-Hua Chen,[3] and Hong-Lin Chan [1]*

[1]*Institute of Bioinformatics and Structural Biology & Department of Medical Sciences, National Tsing Hua University, Hsinchu, Taiwan*

[2]*Department of Applied Science, National Hsinchu University of Education, Hsinchu, Taiwan*

[3]*Department of Biomedical Materials, Material and Chemical Research Laboratories, Industrial Technology Research Institute, Hsinchu, Taiwan*

Within ultraviolet radiation, ultraviolet B (UVB) is the most energetic and damaging to humans. At the protein level, UVB irradiation downregulates the expression of antioxidant enzymes leading to the accumulation of reactive oxygen species (ROS). Due to lacking of a global analysis of UVB-modulated corneal proteome, we investigate in vitro the mechanism of UVB-induced corneal damage to determine whether hyaluronic acid (HA) is able to reduce UVB irradiation-induced injury in human corneal epithelial cells. Accordingly, human corneal epithelial cell lines (HCE-2) were irradiated with UVB, followed by incubation with low molecular weight HA (LMW-HA, 100 kDa) or high molecular weight HA (HMW-HA, 1,000 kDa) to investigate the physiologic protection of HMW-HA in UVB-induced corneal injury, and to perform a global proteomic analysis. The data demonstrated that HA treatment protects corneal epithelial cells in the UVB-induced wound model, and that the molecular weight of HA is a crucial factor. Only HMW-HA significantly reduces the UVB-induced cytotoxic effects in corneal cells and increases cell migration and wound-healing ability. In addition, proteomic analysis showed that HMW-HA might modulate cytoskeleton regulation, signal transduction, biosynthesis, redox regulation, and protein folding to stimulate wound healing and to prevent these UVB-damaged cells from cell death. Further studies evidenced membrane-associated progesterone receptor component 1 (mPR) and malate dehydrogenase (MDH2) play essential roles in protecting corneal cells from UVB irradiation. This study reports on UVB-modulated cellular proteins that might play an important role in UVB-induced corneal cell injury and show HMW-HA to be a potential substance for protecting corneal cells from UVB-induced injury. Environ. Mol. Mutagen. 54:429–449, 2013.

Key words: UVB; cornea; hyaluronic acid; proteomics; DIGE

INTRODUCTION

Ultraviolet B (UVB) irradiation is one of the most common corneal injuries among the most severe ocular accidents. A recent report shows that the cornea absorbs more than 90% of UVB, and excessive exposure to UVB might induce edema, photokeratitis, photo-ophthalmia, and epithelial damage [Downes et al., 1994; Kolozsvari

Abbreviations: BSA, bovine serum albumin; DIGE, differential gel electrophoresis; FCS, fetal calf serum; HA, hyaluronic acid; MDH2, malate dehydrogenase; mPR, membrane-associated progesterone receptor component 1; NP-40, Nonidet P-40; TFA, trifluoroacetic acid; UVB, ultraviolet-B.Grant sponsor: National Science Council, Taiwan; Grant number: 100-2311-B-007-005 and 101-2311-B-007-011.
Grant sponsor: National Tsing Hua University; Grant number: 100N2723E1, 99N2908E1 and 100N2051E1.

*Correspondence to: Hong-Lin Chan, Institute of Bioinformatics and Structural Biology & Department of Medical Sciences, National Tsing Hua University, Hsinchu, Taiwan. E-mail: hlchan@life.nthu.edyu.tw

Dr. H.L. Chan designed the study and prepared the manuscript draft. J.M. Li and C.L. Wu performed the experiments. Dr. H.C. Chou performed data analysis and prepared draft figures and tables. All authors approved the final manuscript.

Received 28 August 2012; provisionally accepted 20 May 2013; and in final form 21 May 2013

DOI 10.1002/em.21794

Published online 27 June 2013 in
Wiley Online Library (wileyonlinelibrary.com).

et al., 2002]. In UVB-induced cell damage, UVB irradiation has been shown to generate excessive levels of reactive oxygen species (ROS), which might damage DNA and activate both extrinsic and intrinsic cell-death pathways by activating cell death membrane receptors, the caspase-8 pathway, mitochondrial death signals, and the caspase-9 pathway [Okada and Mak, 2004; Pauloin et al., 2009]. In the molecular mechanism, corneal irradiation with UVB results in the downregulation or inactivation of antioxidant enzymes, including superoxide dismutase, glutathione peroxidase, and catalase in the corneal epithelium, which might contribute to corneal damage from UVB through ROS accumulation [Cejkova et al., 2000; Lodovici et al., 2003]. In contrast, repeated irradiation with UVB has been reported to overexpress nitric oxide (NO) synthase, resulting in NO production, peroxynitrite formation, and lipid peroxidation [Cejkova et al., 2005]. However, a global analysis of a UVB-modulated corneal proteome in previous studies is lacking.

HA serves as one of the major extracellular matrix components upon connective tissues and is reported abundant inside the vitreous body of the eye. It is biosynthesized as large 1,000 kDa disaccharide chains and is then gradually degraded in the extracellular matrix to give intermediate size HA (10–100 kDa) or even small fragments (<1 kDa) [Pauloin et al., 2008]. HA has been described to functionally modulate cell migration, wound healing and cancer cell metastasis [Toole, 2004] and the presence of endogenous HA was observed in various diseased human corneas, including alkali-burn wounded corneas [Fitzsimmons et al., 1994; Chung et al., 1996]. In recent works, HMW-HA has shown to decrease benzalkonium chloride- and UVB-induced apoptosis in human corneal epithelial cells [Pauloin et al., 2008, 2009] and enable to speed up wound healing of corneal epithelium in diabetic rats [Yang et al., 2010], yet the role of various forms of HA on mechanisms of corneal wound healing process following alkali burns has not been known.

In this study, the cellular targets of UVB-irradiation of corneal cells were monitored by lysine-labeling 2D-DIGE [Chan et al., 2005, 2006; Huang et al., 2010; Lai et al., 2010; Chen et al., 2011a,b; Hung et al., 2011; Chou et al., 2010, 2012; Wu et al., 2012]. These strategies combined with MALDI-TOF MS were used to determine whether cellular protein abundance was altered. The results demonstrated a number of differentially labeled proteins that were identified from 2-DE by MS. Subsequently, we examined the protective ability of HA in UVB-irradiated human corneal epithelial cells by performing biological assays including cell proliferation and wound healing. Our data demonstrated that the presence of HA may have a therapeutic role to suppress UVB injury and the molecular weight of HA is a crucial factor in corneal cell protection. Moreover, proteomic analysis of the effects of HA on corneal UVB-irradiation was also evaluated in this study.

MATERIALS AND METHODS

Chemicals and Reagents

Generic chemicals were purchased from Sigma-Aldrich (St. Louis), while reagents for 2D-DIGE were purchased from GE Healthcare (Uppsala, Sweden). All primary antibodies were purchased from GeneTex (Hsinchu, Taiwan) and anti-mouse and anti-rabbit secondary antibodies were purchased from GE Healthcare (Uppsala, Sweden). The LMW-HA and HMW-HA used in this study were both medical grade (listed in European Pharmacopoeia) and purchased from Shiseido Co. (Tokyo, Japan). These HAs contain less than 1% protein content and less than 0.0003 IU/mg bacterial endotoxins. All the chemicals and biochemicals used in this study were of analytical grade.

Cell Line and Cell Cultures

The human corneal epithelial cell line HCE-2 was a gift from National Taiwan University Hospital, Taiwan. The cell line was maintained in Dulbecco's Modified Eagle's medium and F-12 medium (DMEM/F-12) supplemented with 10% fetal calf serum, L-glutamine (2 mM), streptomycin (100 μg per mL), penicillin (100 IU per mL), epidermal growth factor (20 ng per mL) (all from Gibco-Invitrogen Corp., UK), insulin (10μg per mL) (Sigma) and hydrocortisone (0.5μg per mL) (Sigma). Cells were incubated at 37°C and 5% CO_2.

MTT Cell Proliferation Assay

HCE-2 cells growing exponentially were trypsinized and seeded at a density of 5,000 cells per well into 96-well plates. After washing with PBS three times, the HCE-2 cells were transiently irradiated with indicated doses of UVB or left untreated followed by incubation in serum-free medium for 24 hr. The detail MTT procedure has been described in our previous publication [Chou et al., 2012].

Scratch Wound Healing Assay

Exponentially growing HCE-2 cells were trypsinized and seeded at a density of 30,000 cells per well into 24-well plates for 24 hr incubation (~90% confluence). The scratch wounds were made by a sterile 200 μL pipette tip through a pre-marked line. After removal of the resulting debris from five lineal scratches, HCE-2 monolayer was subsequently treated with indicated doses of UVB and rinsed three times with PBS followed by incubated with serum-free medium for 24 hr. The wound areas were displayed by taking images just above the interchanges between scratched wound areas and pre-marked lines.

Sample Preparation and 2D-DIGE-Based Proteomic Analysis

The detail experimental procedures have been described in our previous publications [Lai et al., 2010]. Briefly, HCE-2 cells in normal growth medium at ~80% confluence were used for proteomic analysis. HCE-2 cells with various treatments or left without treatment were lysed with 2-DE lysis buffer. Before performing 2D-DIGE analysis, protein samples were labeled with *N*-hydroxy succinimidyl ester-derivatives of the cyanine dyes Cy2, Cy3, and Cy5. Protein sample (150 μg) was minimally labeled with 375 pmol of either Cy3 or Cy5 for comparison on the same 2-DE. In contrast, to facilitate image matching and cross-gel statistical comparison, a pool of all samples was also prepared and labeled with Cy2 at a molar ratio of 2.5 pmol Cy2 per μg of protein as an internal standard for all gels. Thus, the triplicate samples and the internal standard could be run and quantify on multiple 2-DE. Afterward, the fluorescence 2-DE were scanned directly between the low fluorescent glass plates using an Ettan DIGE Imager and gel analysis was

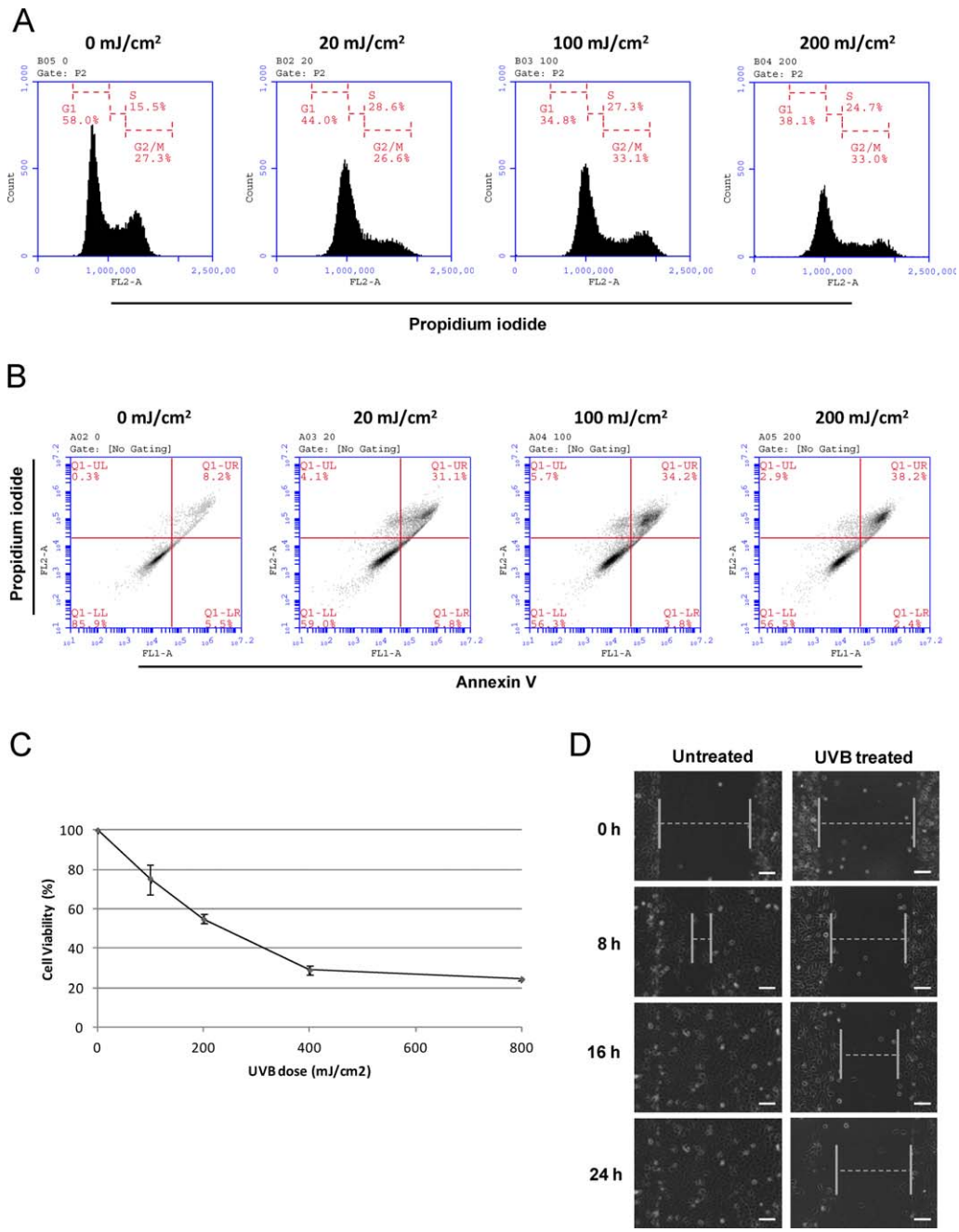

Fig. 1. UVB-induced alterations on cell cycle, cell apoptosis, cell proliferation and wound closure ability in HCE-2 cells. (**A**) Cell cycle analysis following UVB irradiation of HCE-2 cells for indicated doses. The percentage of cells at each stage of the cell cycle was analyzed by flow cytometry after DNA staining with propidium iodide. Propidium iodide fluorescence intensity is directly proportional to the quantity of DNA per nuclei. The G1 cell cycle phase is the primary peak, the S phase fraction is the area between the G1 and G2/M peaks, and the rightmost peak is the G2/M fraction. (**B**) HCE-2 cells were irradiated with indicated doses of UVB or left untreated for 24 hr. After irradiation, 10^6 cells were incubated with Alexa Fluor 488 and propidium iodide in 1× binding buffer at room temperature for 15 min, and then stained cells were analyzed by flow cytometry. Annexin V is presented in *x*-axis as FL1-H, and propidium iodide is presented in *y*-axis as FL2-H. LR quadrant indicates the percentage of early apoptotic cells (Annexin V positive cells), and UR quadrant indicates the percentage of late apoptotic cells (Annexin V positive and propidium iodide positive cells). (**C**) MTT-based cell proliferation assays were performed where 10,000 HCE-2 cells were plated into 96-well plates in medium containing 10% FBS. After 24 hr, the cells were irradiated with the indicated doses of UVB. Cells were incubated with MTT and then DMSO added and the plates shaken for 20 min followed by measurement of the absorbance at 540 nm. Values were normalized against untreated samples and are the average of 4 independent measurements ± the standard deviation. (**D**) The wound HCE-2 cells were treated with 200 mJ/cm^2 UVB. The wound healing of HCE-2 cells were photographed at the times indicated. Each treatment condition has been performed at least three times. [Color figure can be viewed in the online issue, which is available at wileyonlinelibrary.com.]

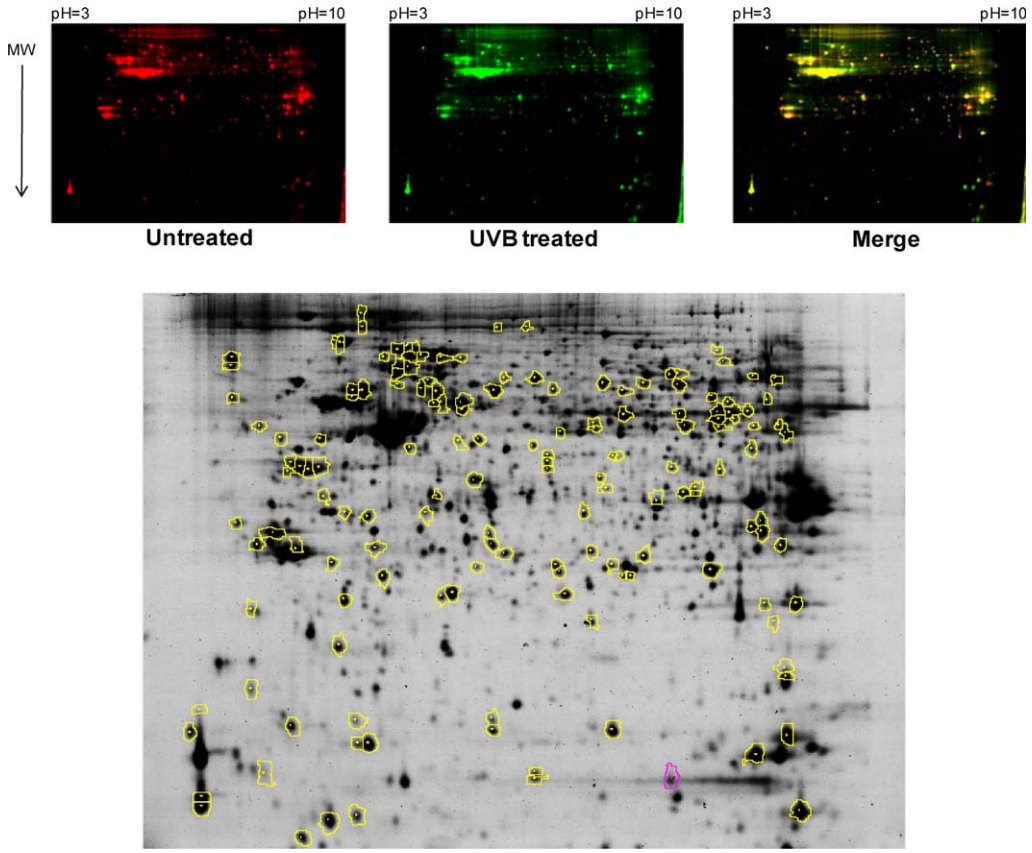

Fig. 2. 2D-DIGE analysis of UVB-dependent differentially expressed proteins in HCE-2 cells. UVB-irradiated HCE-2 cells were lysed and arranged for a triplicate 2D-DIGE experiment. Protein samples (150 μg each) were labeled with Cy-dyes and separated using 24 cm, pH 3-10 nonlinear IPG strips. The 2D-DIGE images of the protein samples from untreated and 200 mJ/cm^2 UVB-irradiated HCE-2 cells were shown as well as overlaid pseudo-colored image processed with ImageQuant Tool (GE Healthcare) (top images). The differentially expressed identified proteins with greater than 1.5-fold differences are annotated with circles (bottom image). [Color figure can be viewed in the online issue, which is available at wileyonlinelibrary.com.]

performed using DeCyder 2-D Differential Analysis Software v7.0 (GE Healthcare) to co-detect, normalize and quantify the protein features in the images. Features detected from non-protein sources (e.g. dust particles and dirty backgrounds) were filtered out. Spots displaying a ≧1.5 average-fold increase or decrease in abundance with a P value <0.05 were selected for protein identification.

Protein Staining, In-Gel Digestion, and MALDI-TOF MS Analysis

Colloidal coomassie blue G-250 staining was used to visualize CyDye-labeled protein features in 2-DE followed by excised interested post-stained gel pieces for MALDI-TOF MS identification. The detailed procedures for protein staining, in-gel digestion, MALDI-TOF MS analysis, and the algorithm used for data processing were described in our previous publication [Lai et al., 2010]. The spectrometer was also calibrated with a peptide calibration standard (Bruker Daltonics) and internal calibration was performed using trypsin autolysis peaks at m/z 842.51 and m/z 2211.10. Peaks in the mass range of m/z 800 to 3,000 were used to generate a peptide mass fingerprint that was searched against the Swiss-Prot/TrEMBL database (v57.12) with 513,877 entries using Mascot software v2.2.06 (Matrix Science, London, UK). The following parameters were used for the search: *Homo sapiens*; tryptic digest with a maximum of one missed cleavage; carbamidomethylation of cysteine, partial protein N-terminal acetylation, partial methionine oxidation and partial modification of glutamine to pyroglutamate, and a mass tolerance of 50 ppm. Identification was accepted based on significant MASCOT Mowse scores ($P < 0.05$), spectrum annotation and observed versus expected molecular weight and pI on 2-DE.

Immunoblotting Analysis

Immunoblotting analysis was used to validate the differential abundance of mass spectrometry identified proteins. The detailed experimental procedures were described in our previous reports [Chen et al., 2011a,b; Hung et al., 2011; Lin et al., 2011]. All of primary antibodies used for expression validation were purchased from Genetex (Hsinchu, Taiwan).

Immunofluorescence

The detailed experimental procedures for immunofluorescence analysis was described in our previous reports [Lai et al., 2010].

siRNA Design, Construction, and Transfection

The siRNA against mPR and MDH2 were synthesized by Invitrogen. The targeting sequences 5′-AAU UUG CGG CCU UUG GUC ACA UCG A-3′ and 5′-AGU GAA CUG AGA CUC CCA GUC ACU C-3′ against mPR and sequences 5′-UUC AGG UCC GAG GUA GCC UUU CAC A-3′, 5′-AAU CGU GGC AUU GGU GUU GAA CAG G-3′ and 5′-UAA CGA AGG AAC AUU CCA CAA CAC C-3′ against MDH2

TABLE I. Alphabetic List of Identified Differentially Up-Regulated Proteins After 2D-DIGE Coupled With MALDI-TOF Mass Spectrometry Analysis in HCE-2 Cells in Response to UVB Irradiation

Spot no.	Swiss-prot no.	Protein name	MW	pI	No. matched peptides	MOWSE score	Seq cov. (%)	Subcellular location	Functional classification	UVB treated/ untreated[a]	Matched peptides
1283	P10809	60 kDa heat shock protein, mitochondrial	61,187	5.7	7	74/56	14	Mitochondrion	Protein folding	2.55	R.TVIIEQSWGSPK.VK.GANPVEIR.R
1108	P05386	60S acidic ribosomal protein P1[b]	11,621	4.26	1	91/56 (MS/MS)	14	Cytoplasm	Biosynthesis	1.99	K.AAGVNVEPFWPGLFAK.A
919	O95336	6-phosphogluconolactonase	27,815	5.7	6	104/56	30	Cytoplasm	Carbohydrate metabolism	2.53	R.ELPAAVAPAGPASLAR.WR.WTLGFCDER.L
157	P11021	78 kDa glucose-regulated protein	72,402	5.07	9	93/56	17	Endoplasmic Reticulum	Biosynthesis	3.13	R.ITPSYVAFTPEGER.LK.VTHAVVTVPAYFNDAQR.Q
147	P11021	78 kDa glucose-regulated protein	72,402	5.07	10	121/56	17	Endoplasmic Reticulum	Biosynthesis	3.07	R.VEIIANDQGNR.IR.ITPSYVAFTPEGER.L
1265	P54819	Adenylate kinase isoenzyme 2, mitochondrial[b]	26,689	7.67	1	57/56 (MS/MS)	4	Mitochondrion	Biosynthesis	1.63	K.NGFLLDGFPR.T
490	P06733	Alpha-enolase	47,481	7.01	6	70/56	17	Cytoplasm	Metabolism	2.34	R.AAVPSGASTGIYEALELR.DK.YNQLLR.I
474	P06733	Alpha-enolase	47,481	7.01	9	83/56	22	Cytoplasm	Metabolism	2.14	R.AAVPSGASTGIYEALELR.DR.IGAEVYHNLK.N
468	P06733	Alpha-enolase	47,481	7.01	5	82/56	15	Cytoplasm	Metabolism	2.1	R.AAVPSGASTGIYEALELR.DK.VVIGMDVAASEFFR.S
518	P06733	Alpha-enolase	47,481	7.01	6	77/56	15	Cytoplasm	Metabolism	2.02	R.AAVPSGASTGIYEALELR.DK.LAQANGWGVMVSHR.S
522	P06733	Alpha-enolase	47,481	7.01	8	101/56	20	Cytoplasm	Metabolism	1.9	R.AAVPSGASTGIYEALELR.DR.IGAEVYHNLK.N
547	P06733	Alpha-enolase	47,481	7.01	6	84/56	18	Cytoplasm	Metabolism	1.74	R.AAVPSGASTGIYEALELR.DR.YISPDQLADLYK.S
782	P04083	Annexin A1	38,918	6.57	10	113/56	33	Cell membrane	Signal transduction/ Ca regulation	1.52	K.TPAQFDADELR.AK.GLGTDEDTLIEILASR.T
816	P08758	Annexin A5	35,971	4.94	7	66/56	22	Cell Membrane	Signal transduction/ Ca regulation	1.65	R.GTVTDFPGFDER.AK.GLGTDEESILTLLTSR.S
944	P04632	Calpain small subunit 1	28,469	5.05	6	76/56	14	Cytoplasm/Cell membrane	Signal transduction/ Cytoskeleton remodelling/ Ca regulation	1.97	R.HPDLKTDGFGIDTCR.SK.TDGFGIDTCR.S
206	P27797	Calreticulin	48,283	4.29	6	73/56	19	Endoplasmic Reticulum	Signal transduction/ Ca regulation	2.07	K.EQFLDGDGWTSR.W R.FYALSASFEPFSNK.G
250	P27797	Calreticulin[b]	48,283	4.29	1	115/56 (MS/MS)	2	Endoplasmic Reticulum	Signal transduction/ Ca regulation	1.62	K.EQFLDGDGWTSR.W
722	P48729	Casein kinase I isoform alpha	39,118	9.59	5	57/56	15	Cytoplasm	Cell cycle	1.99	K.AEFIVGGKYK.L R.DIKPDNFLMGIGR.H
1111	P23528	Cofilin-1	18,719	8.22	6	82/56	38	Cytoplasm	Cell motility/ Ca regulation	1.67	K.AVLFCLSEDKK.NK.EILVGDVGQTVDDPYATFVK.M
1267	Q9H223	EH domain-containing protein 4	61,365	6.33	5	62/56	12	Cell membrane	Transport	2.15	R.DIQSLPQK.AR.EYQISAGDFPEVK.A
754	P29692	Elongation factor 1-delta	31,217	4.9	7	85/56	32	Cytoplasm	Biosynthesis	1.84	K.SLAGSSGPGASSGTSGDHGELVVR.IR.IASLEVENQSLR.G
1258	P26641	Elongation factor 1-gamma	50,429	6.25	7	82/56	15	Cytoplasm	Biosynthesis	1.59	M.AAGTLYTYPENWR.AK.ALIAAQYSGAQVR.V
542	P49411	Elongation factor Tu, mitochondrial	49,852	7.26	11	111/56	30	Mitochondrion	Biosynthesis	1.69	R.DKPHVNVGTIGHVDHGK.TK.KYEEIDNAPEER.A
914	P30040		29,032	6.77	6		21/3		Protein folding	1.64	K.LDKESYPVFYLFR.DK.ESYPVFYLFR.D

TABLE I. (continued).

Spot no.	Swiss-prot no.	Protein name	MW	pI	No. matched peptides	MOWSE score	Seq cov. (%)	Subcellular location	Functional classification	UVB treated/ untreated[a]	Matched peptides
		Endoplasmic reticulum protein ERp29[b]				74/56 82/56 (MS/MS)		Endoplasmic Reticulum			
893	P30040	Endoplasmic reticulum protein ERp29[b]	29,032	6.77	5	62/5672/56 (MS/MS)	20/3	Endoplasmic Reticulum	Protein folding	1.62	K.FDTQYPYGEK.QK.LDKESYPVFYLFR.D
1118	Q9GZV4	Eukaryotic translation initiation factor 5A-2[b]	17,124	5.38	1	110/56 (MS/MS)	7	Nucleus	Biosynthesis	2.06	
182	Q96AE4	Far upstream element-binding protein 1	67,690	7.18	8	95/56	13	Nucleus	Gene regulation	2.13	K.VPDGMVGFIIGR.GK.IQIAPDSGGLPER.S
1180	P09382	Galectin-1	15,048	5.34	6	90/56	58	Cytoplasm	Cell-cell interaction	1.9	K.DSNNLCLHFNPR.FR.FNAHGDANTIVCNSK.D
1007	P09211	Glutathione S-transferase P	23,569	5.43	7	101/56	40	Cytoplasm	Redox regulation	2.84	M.PPYTVVYFPVR.GK.FQDGDLTLYQSNTILR.H
993	P09211	Glutathione S-transferase P	23,569	5.43	7	102/56	45	Cytoplasm	Redox regulation	2.46	M.PPYTVVYFPVR.GK.FQDGDLTLYQSNTILR.H
198	P08107	Heat shock 70 kDa protein 1	70,294	5.48	7	70/56	14	Cytoplasm	Protein folding	1.91	R.TTPSYVAFTDTER.LK.NQVALNPQNTVFDAKR.L
32	P34932	Heat shock 70 kDa protein 4	95,096	5.18	10	90/56	15	Cytoplasm	Protein folding	1.53	R.AGGIETIANEYSDR.CR.CTPACISFGPK.N
176	P11142	Heat shock cognate 71 kDa protein	71,082	5.37	7	100/56	14	Cytoplasm	Protein folding	2.84	R.TTPSYVAFTDTER.LK.TVTNAVVTVPAYFNDSQR.Q
1256	P11142	Heat shock cognate 71 kDa protein	71,082	5.37	9	123/56	18	Cytoplasm	Protein folding	1.54	K.VEIIANDQGNR.TR.TTPSYVAFTDTER.L
968	P04792	Heat shock protein beta-1	22,826	5.98	10	92/56	40	Cytoplasm	Protein folding	1.62	R.VPFSLLR.GR.LFDQAFGLPR.L
201	P61978	Heterogeneous nuclear ribonucleoprotein K[b]	51,230	5.39	7	66/56 72/56 (MS/MS)	16/2	Nucleus	Gene regulation	1.87	R.SRNTDEMVELR.IR.TDYNASVSVPDSSGPER.I
231	P14866	Heterogeneous nuclear ribonucleoprotein L[b]	60,719	6.65	8	96/56 56/56 (MS/MS)	16/2	Nucleus	Gene regulation	2.41	R.YYGGGSEGGR.AK.TPASPVVHIR.G
1098	P37235	Hippocalcin-like protein 1	22,413	5.21	6	84/56	32	Cytoplasm	Signal transduction/ Ca regulation	1.92	K.LRPEVLQDLR.EK.IYANFFPYGDASK.F
1246	P00492	Hypoxanthine-guanine phosphoribosyltransferase	24,792	6.21	6	75/56	32	Cytoplasm	Biosynthesis	1.77	R.VFIPHGLIMDR.T.K.FFADLLDYIK.A
339	P12268	Inosine-5'-monophosphate dehydrogenase 2	56,226	6.44	5	65/56	13	Nucleus	Biosynthesis	2.01	R.HGFCGIPITDTGR.MR.LVGIISSR.D
376	P08729	Keratin, type II cytoskeletal 7	51,443	5.5	9	105/56	20	Cytoplasm	Cytoskeleton	2.02	M.SIHFSSPVFTSR.SR.SAYGGPVGAGIR.E
369	P08729	Keratin, type II cytoskeletal 7	51,443	5.5	8	100/56	18	Cytoplasm	Cytoskeleton	1.61	M.SIHFSSPVFTSR.S.R.SAYGGPVGAGIR.E
429	P05787	Keratin, type II cytoskeletal 8	53,671	5.52	9	83/56	21	Cytoplasm	Cytoskeleton	2.16	K.WSLLQQQKTAR.SR.LEGLTDEINFLR.Q
467	P05787	Keratin, type II cytoskeletal 8	53,671	5.52	9	72/56	16	Cytoplasm	Cytoskeleton	1.63	R.SYTSGPGSR.I.K.WSLLQQQKTAR.S
423	P05787	Keratin, type II cytoskeletal 8	53,671	5.52	6	54/56	11	Cytoplasm	Cytoskeleton	1.58	R.QLETLGQEK.L.R.LEGLTDEINFLR.Q
1053	Q04760	Lactoylglutathione lyase	20,992	5.12	8	91/56	30	Cytoplasm	Redox regulation	1.97	K.DFLLQQTMLR.V.K.KSLDFYTR.V
728	Q14847	LIM and SH3 domain protein 1	30,097	6.61	6	66/56	18	Cytoplasm	Cytoskeleton	2.31	K.KPYCNAHYPK.QK.QQSELQSQVR.Y
736	Q14847	LIM and SH3 domain protein 1	30,097	6.61	8	85/56	26	Cytoplasm	Cytoskeleton	2	K.VNCLDKFWHK.AK.KPYCNAHYPK.Q
1262	P40925	Malate dehydrogenase, cytoplasmic[b]	36,631	6.91	6	70/5694/56 (MS/MS)	203	Mitochondrion	TCA cycle	1.53	K.ENFSCLTR.LK.NVIIWGNHSSTQYPDVNHAK.V
1025	O00264	Membrane-associated progesterone receptor component 1	21,772	4.56	5	77/56	16	Cell membrane	Receptor	1.84	R.DFTPAELR.RR.DFTPAELRR.F
827	Q15691	Microtubule-associated protein RP/EB family member 1	30,151	5.02	6	86/56	26	Cytoplasm	Cytoskeleton	3.18	M.AVNVYSTSVTSDNLSR.HK.LEHEYIQNFK.I
1102	P19105		19,839	4.67	8	97/56	57	Cytoplasm	Cell motility	2.05	K.LNGTDPEDVIR.NR.NAFACFDEEATGTIQEDYLR.E

TABLE I. (continued).

Spot no.	Swiss-prot no.	Protein name	MW	pI	No. matched peptides	MOWSE score	Seq cov. (%)	Subcellular location	Functional classification	UVB treated/ untreated[a]	Matched peptides
		Myosin regulatory light chain MRLC3									
1021	Q06830	Peroxiredoxin-1	22,324	8.27	7	75/56	27	Cytoplasm	Redox regulation	1.85	K.IGHPAPNFK.A.R.TIAQDYGVLK.A
1016	Q06830	Peroxiredoxin-1	22,324	8.27	7	90/56	27	Cytoplasm	Redox regulation	1.65	K.IGHPAPNFK.AR.TIAQDYGVLK.A
955	Q13162	Peroxiredoxin-4	30,749	5.86	6	63/56	20	Cytoplasm	Redox regulation	1.63	R.TREEECHFYAGGQVYPGEASR.VR.EEECHFYAG GQVYPGEASR.V
584	P00558	Phosphoglycerate kinase 1	44,985	8.3	5	66/56	18	Cytoplasm	Carbohydrate metabolism	1.61	K.NNQITNNQR.I.K.LGDVYVNDAFGTAHR.A
933	P18669	Phosphoglycerate mutase 1[b]	28,900	6.67	7	93/5664/56 (MS/MS)	354	Cytoplasm	Carbohydrate metabolism	3.91	R.HGESAWNLENR.F.R.FSGWYDADLSPAGHEEAK.R
1174	P07737	Profilin-1	15,216	8.44	6	73/56	40	Cytoplasm	Cell motility	1.97	K.TFVNITPAEVGVLVGKDR.SR.DSLLQDGEFSMDLR.T
379	P30101	Protein disulfide-isomerase A3	57,146	5.98	11	107/56	21	Endoplasmic Reticulum	Protein folding	1.69	R.LAPEYEAAATR.L.K.QAGPASVPLR.T
1038	Q99497	Protein DJ-1	20,050	6.33	5	62/56	25	Cytoplasm	Redox regulation	2.03	K.VTVAGLAGKDPVQCSR.D.K.EILKEQENR.K
594	Q15293	Reticulocalbin-1	38,866	4.86	6	60/56	18	Endoplasmic Reticulum	Signal transduction/ Ca regulation	1.82	K.TFDQLTPDESK.E.K.TFDQLTPDESKER.L
289	P31948	Stress-induced-phosphoprotein 1	63,227	6.4	10	98/56	16	Cytoplasm	Protein folding	2.03	K.LDPHNHVLYSNR.S.R.KAAALEFLNR.F
283	P31948	Stress-induced-phosphoprotein 1	63,227	6.4	7	77/56	10	Cytoplasm	Protein folding	1.83	K.LDPHNHVLYSNR.S.R.KAAALEFLNR.F
341	P78371	T-complex protein 1 subunit beta	57,794	6.01	8	73/56	19	Cytoplasm	Protein folding	1.97	M.ASLSLAPVNIFK.A.K.IHPQTIIAGWR.E
338	P40227	T-complex protein 1 subunit zeta	58,444	6.23	6	62/56	9	Cytoplasm	Protein folding	1.56	R.AQAALAVNISAAR.G.R.GLQDVLR.T
1238	Q6DKK2	Tetratricopeptide repeat protein 19	42,715	5.57	5	60/56	14	Mitochondrion	Cell cycle	1.85	R.LLSWSLGRGFLR.A.K.QEDNAIIEISLK.L
676	Q6DKK2	Tetratricopeptide repeat protein 19	42,715	5.57	6	62/56	14	Mitochondrion	Cell cycle	1.64	R.LLSWSLGRGFLR.A.K.AITYTYDLMANLAFIR.G
1000	P30048	Thioredoxin-dependent peroxide reductase, mitochondrial[b]	28,017	7.67	2	78/56 (MS/MS) 58/56 (MS/MS)	54	Mitochondrion	Redox regulation	1.85	
1243	P37802	Transgelin-2	22,548	8.41	8	98/56	41	Cytoplasm	Unknown	4.69	R.GPAYGLSR.E R.DDGLFSGDPNWFPKK.S
964	P60174	Triosephosphate isomerase	26,938	6.45	7	103/56	39	Cytoplasm	Carbohydrate metabolism	2.35	K.FFVGGNWK.M. K.VPADTEVVCAPPTAYIDFAR.Q
1252	P61088	Ubiquitin-conjugating enzyme E2 N	17,184	6.13	5	70/56	23	Nucleus	Gene regulation	2.11	K.IYHPNVDK.L.K.DKWSPALQIR.T

[a]Average ratio of differential expression ($P < 0.05$) between UVB-irradiation (200 mJ/cm^2) and untreated cells calculated from triplicate gels. Proteins where the changes between UVB irradiation/untreated are significantly greater than 1.5-fold differences are listed in this table.

[b]These proteins have been identified by MALDI-TOF/TOF MS. The parameters (sequence coverages, MASCOT values, matched peptide numbers, and matched peptide sequences) are obtained from MALDI-TOF/TOF MS sequence analysis.

TABLE II. Alphabetic List of Identified Differentially Down-Regulated Proteins After 2D-DIGE Coupled With MALDI-TOF Mass Spectrometry Analysis in HCE-2 Cells in Response to UVB Irradiation

Spot no.	Swiss-prot no.	Protein name	MW	pI	No. matched peptides	MOWSE score	Seq cov. (%)	Subcellular location	Functional classification	UVB treated/ untreated[a]	Matched peptides
872	P62258	14-3-3 protein epsilon	29,326	4.63	8	74/56	27	Cytoplasm	Signal transduction	−2.04	K.LAEQAER.YK.LICCDILDVLDK.H
907	P61981	14-3-3 protein gamma	28,456	4.8	7	63/56	23	Cytoplasm	Signal transduction	−1.56	R.LAEQAER.YK.NVTELNEPLSNEER.N
393	Q16658	Fascin	55,123	6.84	8	85/56	16	Cytoplasm	Cell motility	−2.21	K.YLTAEAFGFK.VR.FLIVAHDDGR.W
424	P00367	Glutamate dehydrogenase 1, mitochondrial	61,701	7.66	6	71/56	13	Mitochondrion	Metabolism	−1.69	R.DDGSWEVIEGYR.AK.LQHGSILGFPK.A
752	P62873	Guanine nucleotide-binding protein G(I)/G(S)/G(T) subunit beta-1	38,151	5.6	8	99/56	22	Cytoplasm	Signal transduction	−1.57	K.ACADATLSQITNNIDPVGR.IK.IY AMHWGTDSR.L
837	P63244	Guanine nucleotide-binding protein subunit beta-2-like 1	35,511	7.6	7	104/56	28	Cell Membrane	Signal transduction	−2.53	R.DETNYGIPQR.AR.LWDLTTGTTTR.R
867	P63244	Guanine nucleotide-binding protein subunit beta-2-like 1	35,511	7.6	7	104/56	28	Cell Membrane	Signal transduction	−2.56	R.DETNYGIPQR.AR.LWDLTTGTTTR.R
322	P08729	Keratin, type II cytoskeletal 7	51,443	5.5	6	62/56	15	Cytoplasm	Cytoskeleton	−1.5	R.EVTINQSLLAPLR.LR.LPDIFEAQIAGLR.G
555	P04181	Ornithine aminotransferase, mitochondrial	48,846	6.57	7	84/56	20	Mitochondrion	Biosynthesis	−2.27	K.TVQGPPTSDDIFER.EK.YGAHNYHPLPVALER.G
1248	P30041	Peroxiredoxin-6	25,133	6	6	84/56	31	Cytoplasm	Redox regulation	−3.08	M.PGGLLLGDVAPNFEANTTVGR.IR.DFTP VCTTELGR.A
539	P00558	Phosphoglycerate kinase 1	44,985	8.3	5	62/56	14	Cytoplasm	Carbohydrate metabolism	−1.66	K.NNQITNNQR.IK.NNQITNNQRIK.A
878	P61289	Proteasome activator complex subunit 3	29,602	5.69	6	72/56	22	Proteasome	Protein degradation	−1.55	R.RLDECEEAFQGTK.VR.TVESEAASYLDQISR.Y
903	P25788	Proteasome subunit alpha type-3	28,643	5.19	5	70/56	25	Proteasome	Protein degradation	−2.11	K.AVENSSTAIGIR.CK.LYEEGSNKR.L
1037	P28062	Proteasome subunit beta type-8	30,677	7.63	6	87/56	21	Proteasome	Protein degradation	−1.54	K.FQHGVIAAVDSR.AR.ASAGSYISALR.V
305	P34897	Serine hydroxymethyltransferase, mitochondrial	56,414	8.76	11	121/56	21	Mitochondrion	Biosynthesis	−1.51	R.GLELIASENFCSR.AK.TGLIDYNQLALTAR.L
1234	Q13148	TAR DNA-binding protein 43[b]	45,053	5.85	1	141/56 (MS/MS)	4	Nucleus	Biosynthesis	−1.7	
301	P17987	T-complex protein 1 subunit alpha	60,819	5.8	6	60/56	10	Cytoplasm	Protein folding	−2.74	K.IHPTSVISGYR.LR.EQLAIAEFAR.S
1220	Q99832	T-complex protein 1 subunit eta	59,842	7.55	7	79/56	15	Cytoplasm	Protein folding	−2.06	K.QVKPYVEEGLHPQIIIR.AK.LPIGDVATQYFADR.D
361	P23381	Tryptophanyl-tRNA synthetase, cytoplasmic	53,474	5.83	5	68/56	12	Cytoplasm	Biosynthesis	−2.06	R.ATGQRPHHFLR.RK.KPFYLYTGR.G
360	P68363	Tubulin alpha-1B chain	50,804	4.94	12	122/56	33	Cytoplasm	Cytoskeleton	−1.71	R.AVFVDLEPTVIDEVR.TR.QLFHPEQLITGK.E
1284	P68363	Tubulin alpha-1B chain	50,804	4.94	11	114/56	31	Cytoplasm	Cytoskeleton	−1.77	R.AVFVDLEPTVIDEVR.TR.QLFHPEQLITGK.E
340	P68366	Tubulin alpha-4A chain	50,634	4.95	5	71/56	15	Cytoplasm	Cytoskeleton	−2.34	R.AVFVDLEPTVIDEIR.NR.QLFHPEQLITGK.E
390	P07437	Tubulin beta chain	50,095	4.78	7	95/56	19	Cytoplasm	Cytoskeleton	−1.59	R.AILVDLEPGTMDSVR.SK.GHYTEGAELVDSVL DVVR.K
855	P45880	Voltage-dependent anion-selective channel protein 2[b]	32,060	7.49	6	80/56109/56 (MS/MS)	286	Mitochondrion	Transport	−1.94	K.GFGFGLVK.LK.WCEYGLTFTEK.W

[a]Average ratio of differential expression ($P < 0.05$) between UVB-irradiation (200 mJ/cm^2) and untreated cells calculated from triplicate gels. Proteins where the changes between UVB irradiation/untreated are significantly less than −1.5-fold differences are listed in this table.

[b]These proteins have been identified by MALDI-TOF/TOF MS. The parameters (sequence coverages, MASCOT values, matched peptide numbers, and matched peptide sequences) are obtained from MALDI-TOF/TOF MS sequence analysis.

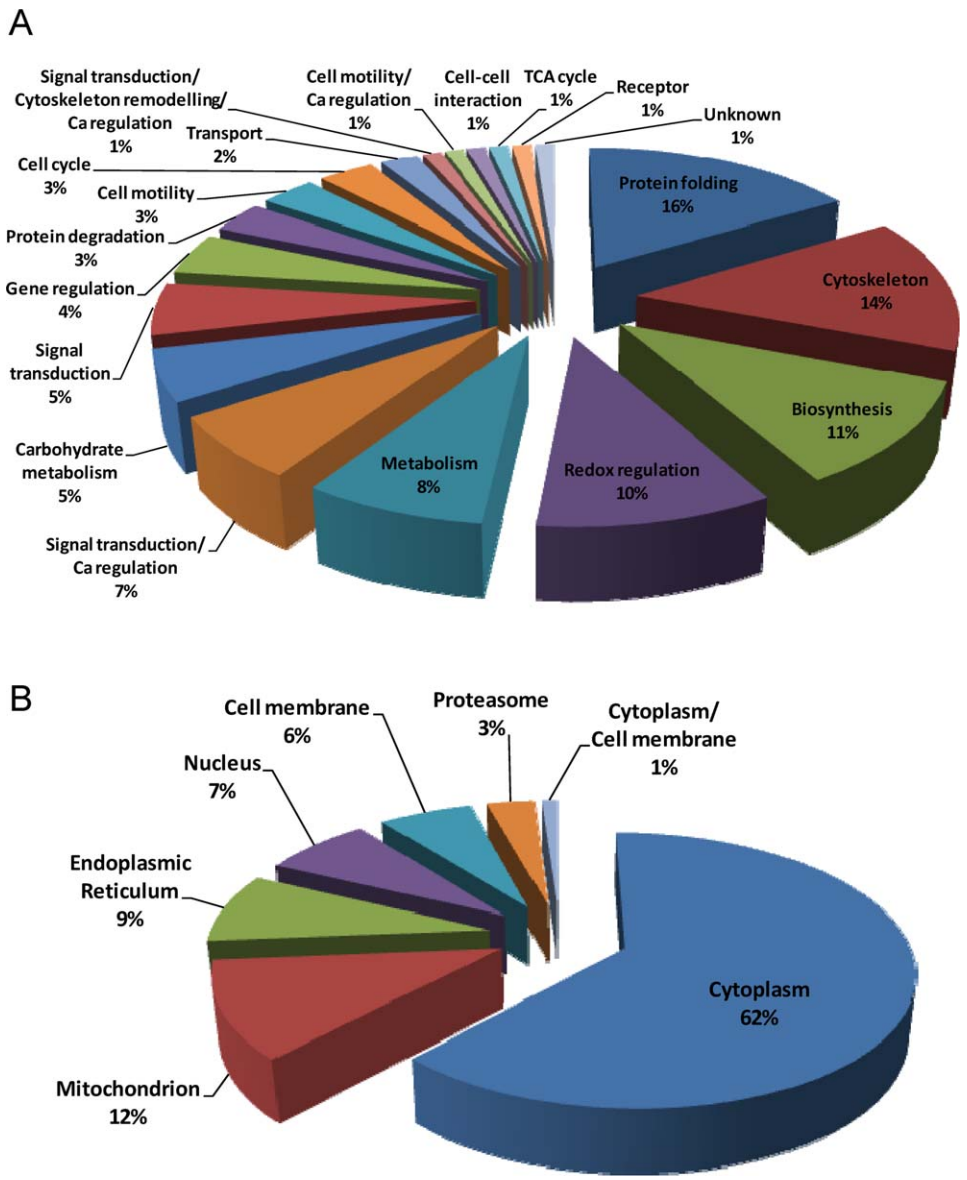

Fig. 3. Percentage of differentially expressed proteins between UVB-treated and UVB-untreated HCE-2 cells according to their biological functions (**A**) and subcellular locations (**B**). [Color figure can be viewed in the online issue, which is available at wileyonlinelibrary.com.]

were designed and verified to be specific by Blast search against the human genome, and sequences of similar GC contents which do not match any known human coding sequence were used for negative control against mPR and MDH2. Transfection was mediated with Lipofectamine RNAiMAX (Invitrogen) according to the manufacturer's instruction. Briefly, cells were transfected with 60 nM of mPR siRNA, 60 nM MDH2 siRNA or the corresponding control (pGCsi-control) in serum free medium containing Lipofectamine RNAiMAX for 4 hr followed by recovered in medium containing 10% FCS for 24 hr. The efficiency of siRNA knockdown was monitored with immunoblotting by using primary antibodies against mPR and MDH2.

Flow Cytometry Analysis for Apoptosis Detection

Annexin-V/propidium iodide (PI) double assay was performed using the Annexin V, Alexa Fluor® 488 Conjugate Detection kit (Life technologies). Following UVB-irradiation, cells were typsinized from culture dish and washed twice with cold PBS; 1×10^6 cells were resuspended in 500 μL binding buffer and stained with 5 μL Alexa Fluor 488 conjugated annexin V according to the manufacturer's instructions. Propidium iodide (PI) (1 μL 100 μg/mL) was added and mixed gently to incubate with cells for 15 min at room temperature in the dark. After incubation period, samples were subjected to FCM analysis in 1 hr. using BD Accuri C6 Flow Cytometry (BD Biosciences, San Jose, CA). The data were analyzed using Accuri CFlow@ and CFlow Plus analysis software (BD Biosciences).

RESULTS

UVB-Induced Shifts in Protein Expression Profiles in Human Corneal Epithelial HCE-2 Cells

To evaluate the UVB effect on human corneal epithelial cells (HCE-2), we exposed these cells to UVB in a

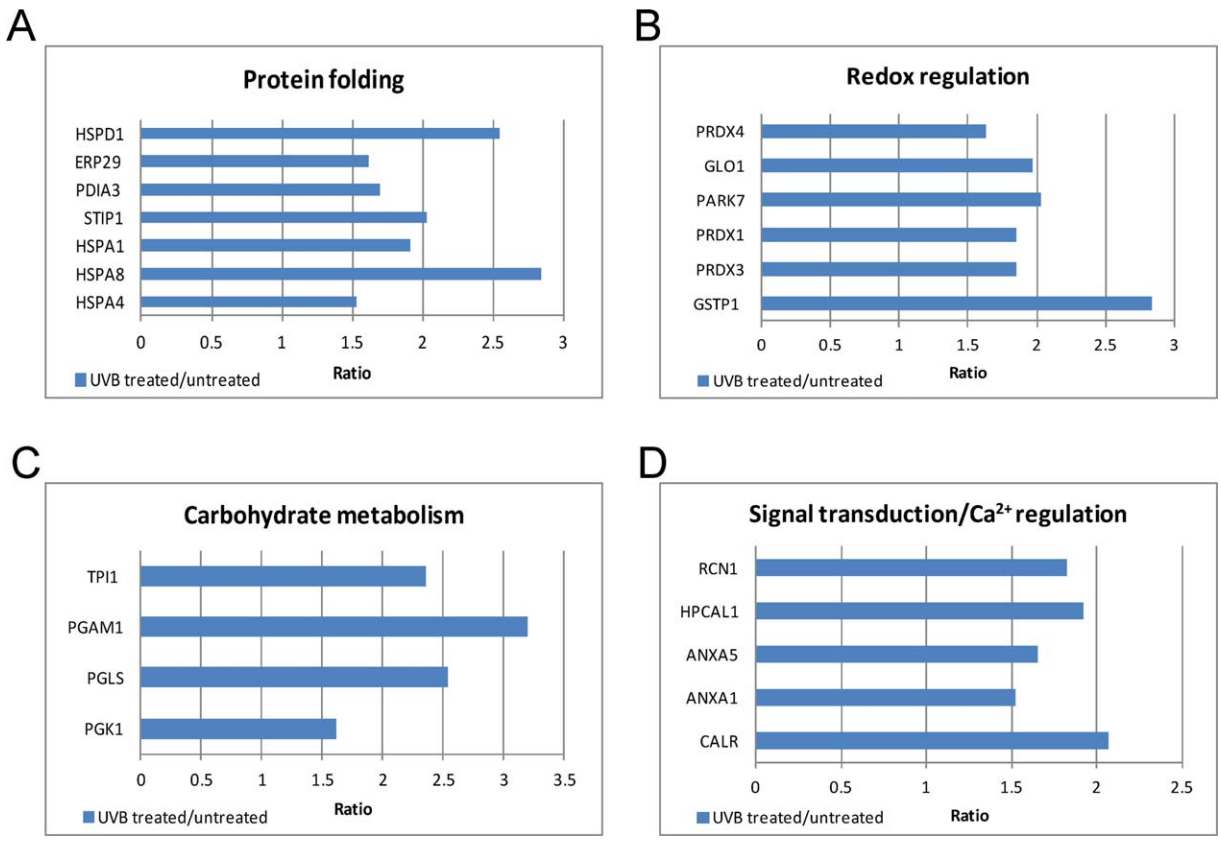

Fig. 4. Expression profiles for differentially expressed proteins potentially contributing to: (**A**) protein folding and (**B**) redox regulation, (**C**) carbohydrate metabolism, and (**D**) signal transduction/calcium regulation in UVB-treated and UVB-untreated HCE-2 cells. The horizontal bars represent fold-changes in protein expression and the vertical axis indicates the identified proteins. Additional details for each protein can be found in Table I. [Color figure can be viewed in the online issue, which is available at wileyonlinelibrary.com.]

range of 0 to 800 mJ/cm^2. We first analyzed the DNA content of UVB-irradiated HCE-2 cells to determine whether UVB irradiation arrests cell cycle progression through propidium iodide staining, followed by flow cytometry analysis. The stained DNA contents of the HCE-2 cells after UVB irradiation demonstrated that 58% of the cells were at G1, 15% were at the S phase, and 27% were at G2/M. The stained DNA contents of the HCE-2 cells following irradiation with 20, 100, and 200 mJ/cm^2 UVB demonstrated that 44%, 34%, and 38% of the cells were at G1, respectively; 28%, 27%, and 24% were at the S phase, respectively; and 26%, 33%, and 33% were at G2/M, respectively, implying a significant cell cycle arrest at the S phase and at the G2/M phase following UVB irradiation (Fig. 1A). In a subsequent study, we used flow cytometry with propidium iodide staining and annexin V-conjugated Alexa Fluor 488 to analyze the percentages of apoptotic HCE-2 cells induced by various doses of UVB irradiation. The total number of apoptotic cells is represented by the number of early apoptotic cells plotted in the LR quadrant and the late apoptotic cells displayed in the UR quadrant of the resulting histograms. We found that UVB irradiation at doses from 0 mJ/cm^2 to 200 mJ/cm^2 increases the percentage of total apoptotic cells (LR + UR) in HCE-2 from 13.7% to 40.6%. Thus, UVB has been shown to directly affect UVB-induced HCE-2 cell apoptosis (Fig. 1B). We performed an MTT assay to determine the UVB-induced cell damage. Exposure to UVB indicated a dose-dependent loss of cell proliferation in HCE-2 (Fig. 1C). At a dose of 200 mJ/cm^2, we detected a significant loss (50%) of cell proliferation at 24 hr. We then studied the UVB effect on the corneal epithelial cell-wound closure. The results demonstrated that 200 mJ/cm^2 UVB reduces the wound closure in HCE-2 cells. Figure 1D shows chronological changes in the areas of 200 mJ/cm^2 UVB-induced epithelial defects. The results also indicate that epithelial wound healing is relatively rapid within 8 hr after wounding in control HCE-2. In contrast, no significant restoration of wound areas was found when HCE-2 cells were irradiated with 200 mJ/cm^2 UVB. These results show that UVB has a considerable effect on corneal epithelial wound healing.

We found HCE-2 cells obtained 24 hr after 200 mJ/cm^2 UVB irradiation or non-irradiation. Two cell lysate samples were analyzed using 2D-DIGE to examine changes in protein expression induced by UVB irradiation. The

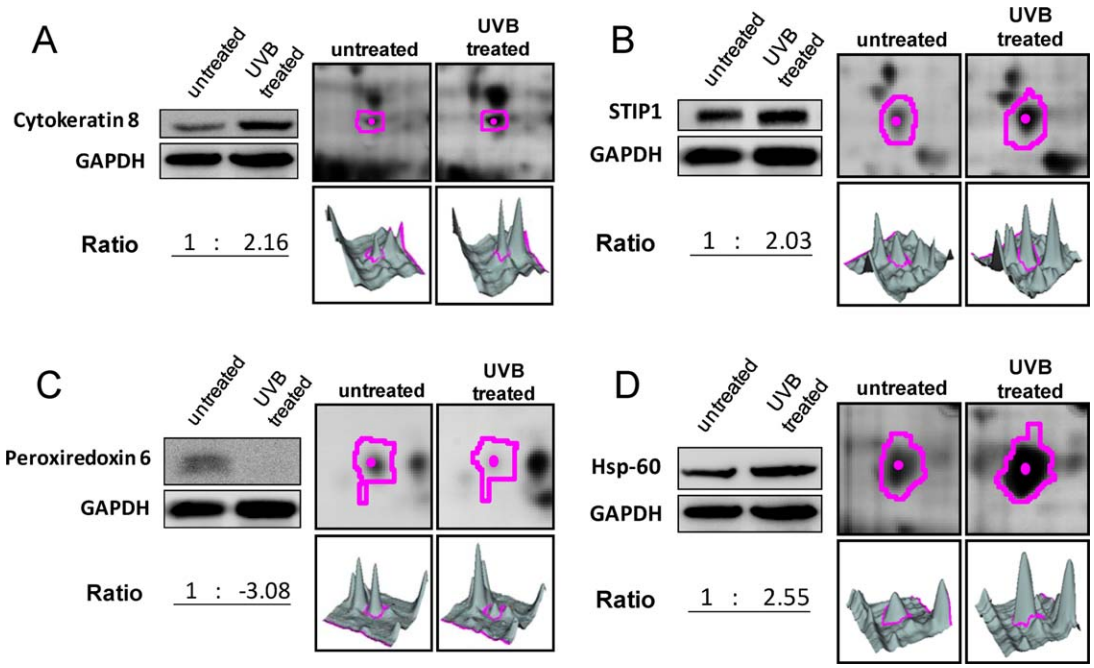

Fig. 5. Representative immunoblotting analyses for selected differentially expressed proteins identified by 2D-DIGE/MALDI-TOF MS for UVB-untreated or -irradiated HCE-2 cells. The levels of identified proteins, (**A**) cytokeratin 8, (**B**) STIP1, (**C**) peroxiredoxin 6, (**D**) HSP-60 in 200 mJ/cm^2 doses of UVB-irradiated HCE-2 cells versus untreated ones were confirmed by immunoblotting. The levels of these proteins were visualized by 2-DE images (top right panels) and three-dimensional spot images (bottom right panels). GAPDH is used as a protein level loading control in immunoblotting. [Color figure can be viewed in the online issue, which is available at wileyonlinelibrary.com.]

analysis detected 1,290 protein spots and 150 protein features that displayed differential expression (≧1.5-fold; $P < 0.05$) between UVB-irradiated HCE-2 cells and the control cells (Fig. 2). The proteins in 95 of these features were subsequently identified by MALDI-TOF MS (Tables I and II). These differentially expressed proteins are located mostly in the cytoplasm, the mitochondria, the endoplasmic reticulum, and the nucleus, and they play a role in protein folding, cytoskeleton regulation, protein biosynthesis, redox regulation, metabolism, and signal transduction (Fig. 3 and Tables I and II).

We further determined numerous potential biological functions of the identified proteins toward UVB-induced cell responses in human corneal epithelial cells by using a Swiss-Prot search combined with KEGG pathway analysis. Our findings demonstrated that UVB treatment upregulates proteins known to regulate protein folding, redox regulation, carbohydrate metabolism, and calcium regulation, but not in the control HCE-2 cells. This result implies the enhanced ability of UVB irradiation in maintaining cellular protein conformation, the redox modification of cellular proteins, cell metabolism, and calcium signaling (Fig. 4). The induced expression of redox-regulated proteins such as peroxiredoxins in UVB-irradiated cells may account for reduced UVB-induced ROS, and our previous observation shows a similar report in UVB-induced skin fibroblast responses [Wu et al., 2012].

To verify the upregulation or downregulation of the identified proteins, we performed immunoblotting analysis on certain proteins that we found modulated by UVB irradiation in HCE-2 cells, compared with the control cells without UVB irradiation (Fig. 5). Among them, we used specific antibodies against cytokeratin 8, STIP1, peroxiredoxin 6, and HSP-60. The immunoblotting results revealed that most of these verified proteins showed the same pattern of expression with 2D-DIGE analysis (Tables I and II). These results also strengthen the validation of 2D-DIGE analysis in this study.

HMW-HA Improves Cell Proliferation and Facilitates Cell Migration and Wound Healing in UVB-Irradiated HCE-2 Cells

In our previous studies, we reported that HA improves cell proliferation and facilitates cell migration and wound healing in alkali-burned injuries in human corneal epithelial cells. To clarify whether HA mediates corneal cell protection against UVB irradiation, we treated UVB-irradiated HCE-2 cells with 0.05% or 0.3% LMW-HA or HMW-HA or left them untreated to investigate the HA effect on corneal epithelial cell proliferation and migration. The results demonstrated that both LMW-HA and HMW-HA improve cell proliferation and the cell migration rate after treatment with an IC_{50} dose of UVB (200

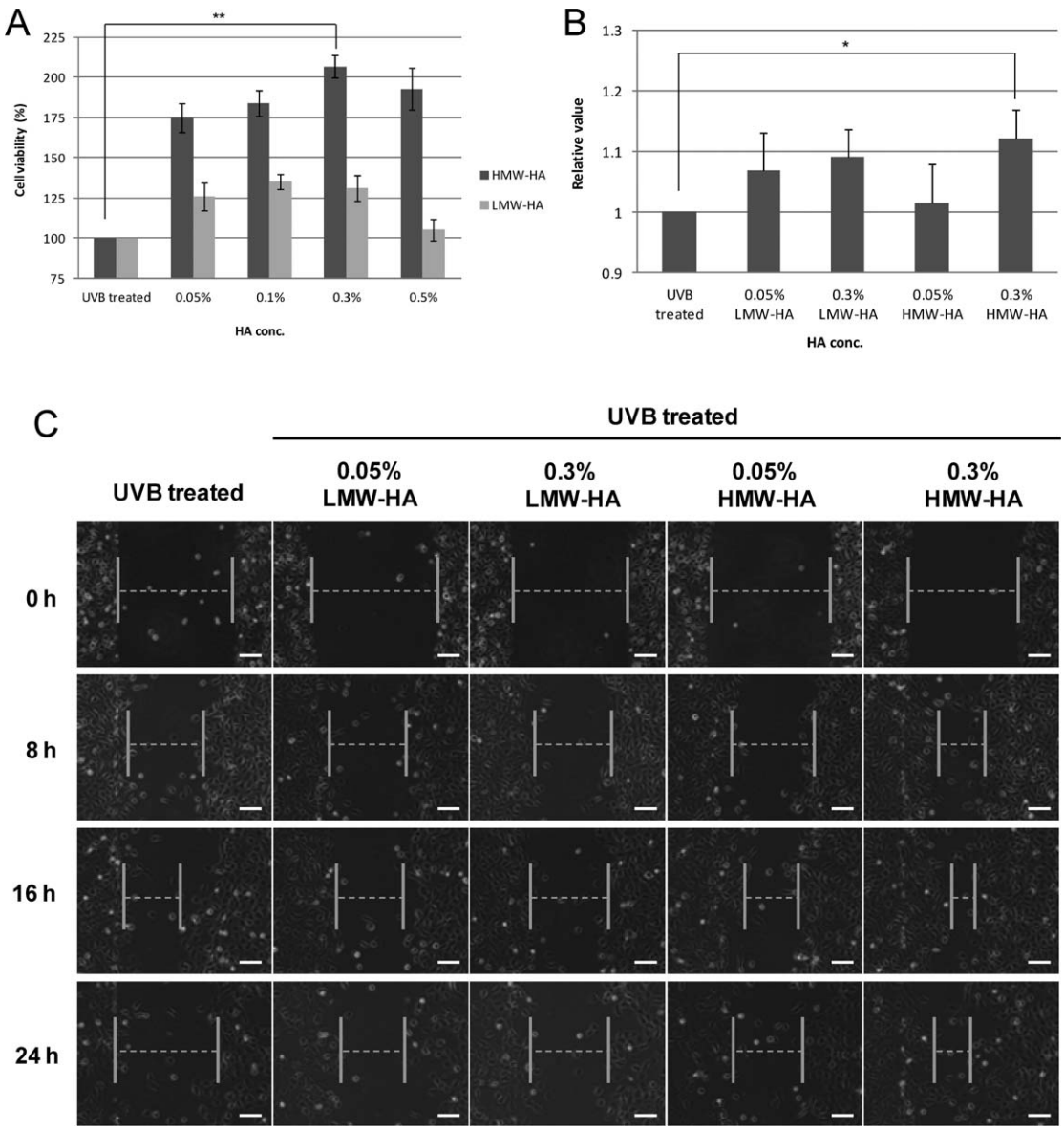

Fig. 6. Effect of LMW-HA and HMW-HA on HCE-2 cell proliferation, migration ability, and wound healing ability after UVB-irradiation. (**A**) HCE-2 cells were incubated in serum free medium and treated with 200 mJ/cm^2 UVB. After three washes with PBS, HCE-2 were incubated in serum free medium containing indicated concentrations of HA or left untreated for 24 hr. Cell proliferation was subsequently determined by MTT cell proliferation assay. Data are mean ± SD of six independent experiments. (**B**) A cloning ring was placed onto the marked circumference inside each well of 24-well tissue culture plates and the HCE-2 cell suspensions were seeded into the cloning ring for an overnight incubation at 37°C before the rings were lifted. The cell monolayers were washed once with PBS and the experiment was initiated by the irradiation of 200 mJ/cm^2 UVB or left untreated followed by washed with PBS. The damaged HCE-2 monolayers were immediately supplied with serum free medium containing indicated concentrations of LMW-HA or HMW-HA for 24 hr before stained with crystal violet for measuring migration pixel areas. Data are mean ± SD of six independent experiments. (**C**) The wound corneal epithelial cells (HCE-2) were treated with indicated concentrations of LMW-HA or HMW-HA in serum free medium or with serum free medium alone after the HCE-2 cells were transiently irradiated with 200 mJ/cm^2 UVB. The wound healing of HCE-2 cells were photographed at the times indicated. Each treatment condition has been performed at least three times.

mJ/cm^2), and HMW-HA showed a considerably higher reduction in cell proliferation compared with LMW-HA treatment (Fig. 6A). However, no significant difference exists in the cell migration ability between LMW-HA and HMW-HA (Fig. 6B). To clarify corneal epithelial wound healing by HA, we examined the effects of various doses of LMW-HA and HMW-HA on wound closure in HCE-2. Figure 6C shows the chronological changes in the areas of 200 mJ/cm^2 UVB-induced epithelial defects, followed by incubation in a serum-free medium containing 0%, 0.05%, or 0.3% LMW-HA or HMW-HA. The results indicated that epithelial wound healing was relatively

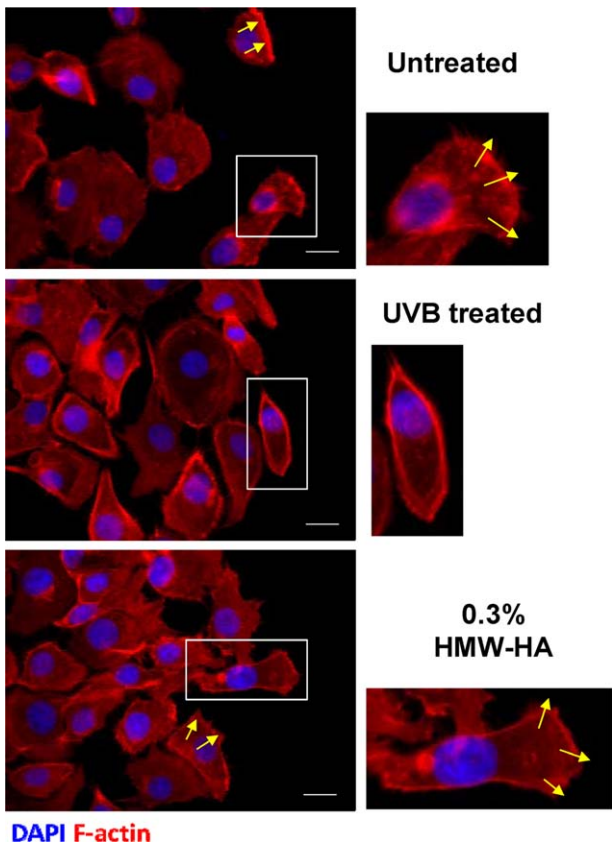

Fig. 7. Immunofluorescence and immunoblotting analysis of morphological, protein localization and protein phosphorylation changes in HCE-2 cells in response to HA treatment and pre-treatment with UVB. The wound HCE-2 cells on cover slips were either left untreated or irradiated with 200 mJ/cm^2 UVB followed by treated with indicated concentrations of HA for indicated periods before fixation and staining for DAPI and F-actin. Each set of three fields were taken using the same exposure and images are representative of six different fields. [Color figure can be viewed in the online issue, which is available at wileyonlinelibrary.com.]

rapid within 8 hr after wounding, and slowed throughout 8 to 24 hr. We observed a positive healing effect in UVB-irradiated HCE-2 cells after treatment with 0.3% HMW-HA. Compared with this condition, wound area restoration decreased significantly when HCE-2 cells were incubated in 0.05% LMW-HA, 0.3% LMW-HA, or 0.05% HMW-HA. These results show that 0.3% HMW-HA has a profound effect on UVB-irradiation-induced corneal epithelial wound healing.

HMW-HA-Modulated Proliferation and Cytoskeletal Proteins Against UVB-Irradiated HCE-2 Cells

The assembly and disassembly of actin networks are the major driving forces of cell movements. Actin polymeration and depolymeration can be modulated by profilin and cofilin, respectively, thereby regulating actin dynamics and cell migration. Further investigation by immunostaining demonstrated that 200 mJ/cm^2 UVB irradiation induced a disruption in the cytoskeletal polarity in the leading edge of HCE-2 cells (Fig. 7). However, an incubation of 0.3% HMW-HA after UVB irradiation promoted F-actin polarity and restored the wound closure (Fig. 7). These observations indicate that actin polymerization/depolymerization modulate peripheral actin organization and HCE-2 polarity after adding 0.3% HMW-HA, presumably leading to an efficient regulation of protrusion dynamics and wound healing of UVB-damaged corneal cells.

Global Analysis of Protein Expression in Untreated or UVB-Irradiated HCE-2 Cells with or without HMW-HA Treatment

To clarify the human corneal epithelial cell response to HMW-HA-mediated protection pathways against UVB irradiation, we performed a 2D-DIGE experiment to examine changes in protein expression in UVB-irradiated HCE-2 cells treated with 0.05% HMW-HA and 0.3% HMW-HA. The analysis revealed more than 85 protein features that displayed differential expression (>1.3-fold; $P < 0.05$) among the 3 conditions (Fig. 8). The proteins in 32 of these features were subsequently identified by MALDI-TOF MS and MS/MS (Tables III and IV). These differentially expressed proteins function primarily in cytoskeleton regulation, signal transduction, biosynthesis, redox regulation, and protein folding (Fig. 9). Numerous identified proteins showed UVB-dependent changes that were partially reversed by HMW-HA treatment. The protein spot 1265 (adenylate kinase isoenzyme 2) was 1.63-fold upregulated by UVB irradiation, but recovered to become 1.36-fold downregulated when these cells were treated with 0.05% HMW-HA (Tables I and II). The protein spot 1102, identified as the myosin regulatory light chain MRLC3, was 2.05-fold upregulated by UVB irradiation, but was significantly downregulated by 1.46-fold when treated with 0.3% HMW-HA (Tables I and II). The protein spot 855, identified as voltage-dependent anion-selective channel protein 1, was 1.94-fold downregulated by UVB irradiation, but was significantly upregulated by 1.4-fold when treated with 0.05% HMW-HA (Tables I and II). These data confirm that HMW-HA partially—if not completely—rescues UVB-induced cell death signals, which are essential for corneal repair processes such as cell proliferation, cell migration, and wound healing.

Evaluating the Roles of mPR and MDH2 on UVB Irradiation in Corneal Cells Using siRNA Knockdown

We found mPR and MDH2 to be overexpressed in UVB-irradiated corneal cells, which are responsible for intracellular signal transduction, energy metabolism, and exchanging reducing equivalents. Thus, we performed knockdown experiments on HCE-2 cells to evaluate the roles of mPR and MDH2 in UVB-irradiated corneal cells.

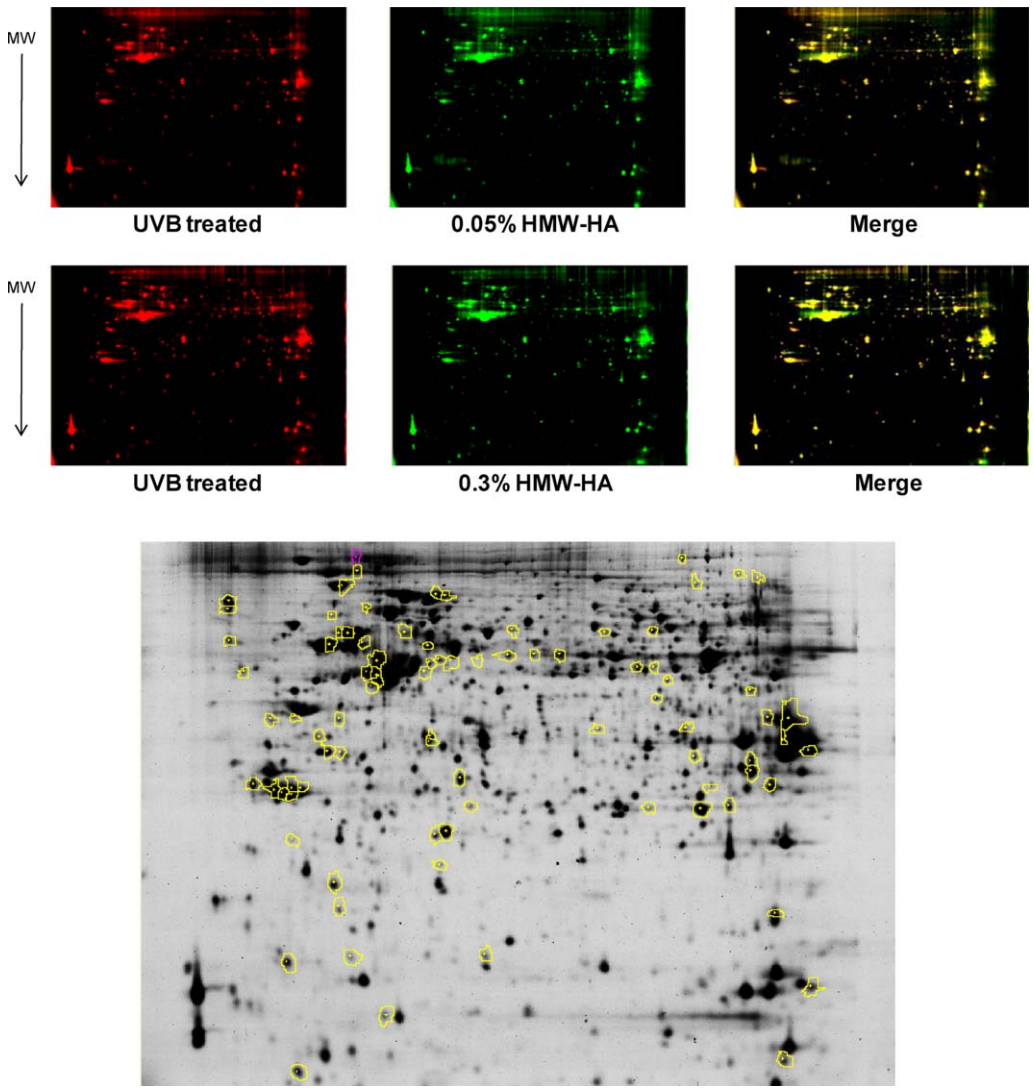

Fig. 8. 2D-DIGE analysis of UVB-induced differential protein expression profiles in human corneal epithelial cells with post-treated by HMW-HA or left untreated. Total cellular proteins (150 μg each) purified from 200 mJ/cm^2 UVB treated HCE-2 cells before treated with indicated concentrations of HMW-HA for 24 hr were labeled with Cy-dyes and separated using 24 cm, pH 3 to 10 nonlinear IPG strips followed by resolved with 12.5% SDS-PAGE. The 2D-DIGE images of UVB-irradiated HCE-2 control and UVB-irradiated HCE-2 cells followed by incubated with indicated concentrations of HMW-HA at appropriate excitation and emission wavelengths were pseudo-colored and overlaid with ImageQuant Tool (top panels). The differentially expressed identified protein features are annotated with circles. [Color figure can be viewed in the online issue, which is available at wileyonlinelibrary.com.]

Immunoblot analysis showed an efficiency that is greater than 90% in the reduction of endogenous mPR and MDH2 protein levels when GAPDH and β-tubulins were the internal standards. We maintained mPR and MDH2 knockdown efficiency for more than 5 days (data not shown). The result indicated that mPR and MDH2 knockdown with 60 mM of siRNA followed by irradiation with the indicated UVB doses leads to UVB dose-dependent reduced proliferation in HCE-2 cells compared with the scramble siRNA transfected controls (Figs. 10A and 10B), implying that mPR and MDH2 play important roles in protecting HCE-2 cells from UVB irradiation.

DISCUSSION

Over the past few decades, the rapid progress of industrial development has resulted in a thinning ozone layer and an increase in solar UVB radiation reaching the earth. The human eye is one of the most sensitive among all organs in its response to external damage. The cornea is located on the outer surface of the eye and suffers more injuries from outside environments. Although the clinical symptoms of UVB-induced damage on the cornea are well characterized, the molecular mechanisms causing this damage require further elucidation. Various approaches have

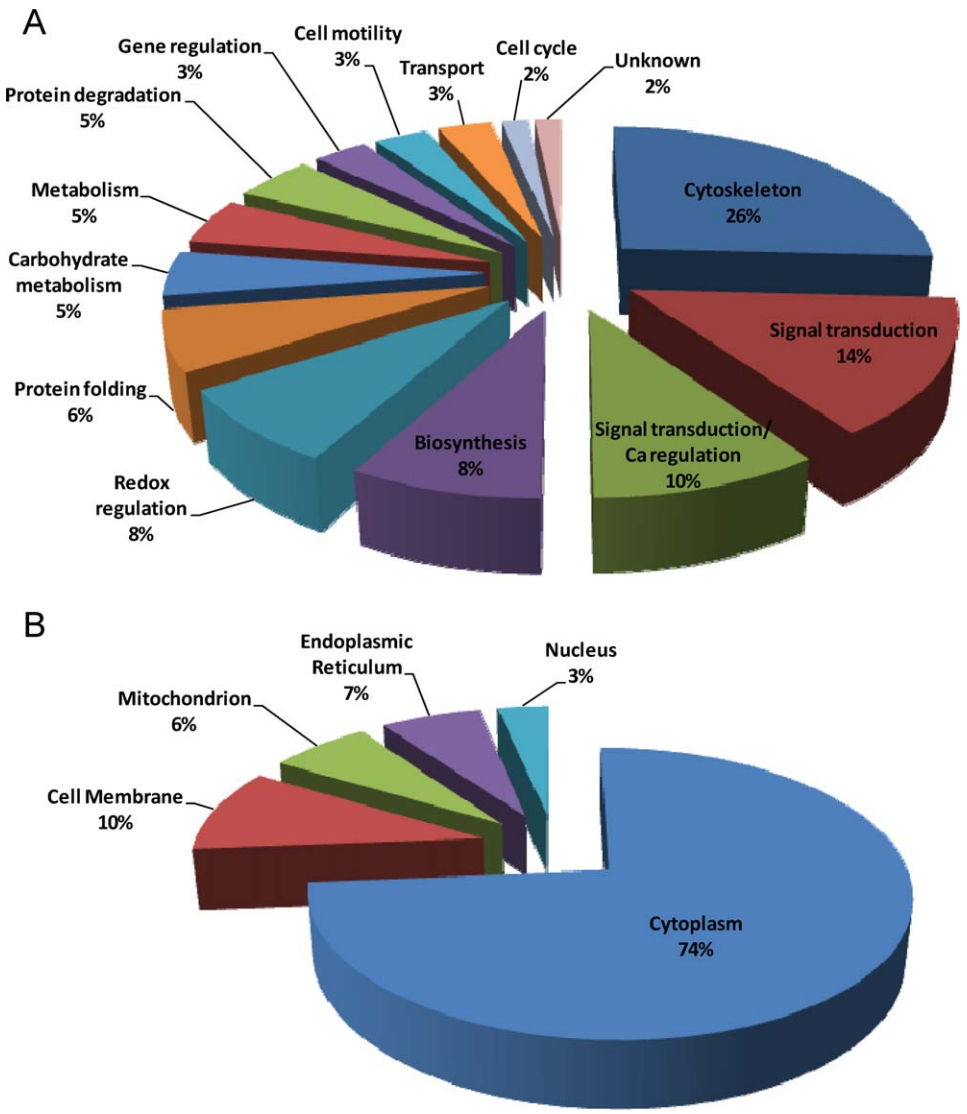

Fig. 9. Percentage of differentially expressed proteins between UVB-irradiated HCE-2 cells with post-treated by HMW-HA or left untreated according to their biological functions (**A**) and subcellular locations (**B**). [Color figure can be viewed in the online issue, which is available at wileyonlinelibrary.com.]

been used to investigate the biological effects of UVB exposure on the cornea, specifically on gene and protein expression levels [Shi et al., 2006; Black et al., 2011; Ardan and Cejkova, 2012]. For example, UVB irradiation of the cornea leads to a deficiency or inactivation in antioxidant enzymes (superoxide dismutase, glutathione peroxidase, and catalase) in the corneal epithelium, which might contribute to corneal damage from UVB and the reactive oxygen products it generates [Cejkova et al., 2000; Lodovici et al., 2003]. In contrast, NO synthase was significantly upregulated in the cornea through repeated UVB irradiation and results in the stimulation of NO production, peroxynitrite formation and lipid peroxidation [Cejkova et al., 2005]. However, no global analysis on the UVB-modulated corneal proteome exists in our knowledge. We thus monitored UVB irradiation-induced alterations in the protein expression of corneal epithelial cells by using lysine-labeling 2D-DIGE. The protein expression profile identified 95 proteins that showed different expression levels in UVB-treated HCE-2 cells compared with non-irradiated cells. Most of these differentially expressed proteins play a role in protein folding and cytoskeleton regulation, implying that UVB might induce corneal protein aggregation, leading to the loss of corneal transparency and a disturbance in wound closure following UVB-induced injury. Our results demonstrated that UVB induced significant cytotoxicity on HCE-2, and we observed a dramatic reduction in cell proliferation (confirmed by at least 3 independent MTT assays), migration ability, and the wound-healing rate following UVB-induced injury. These

TABLE III. Alphabetic List of Identified Differentially Up-Regulated Proteins After 2D-DIGE Coupled With MALDI-TOF Mass Spectrometry Analysis in UVB-Irradiated HCE-2 Cells in Response to HMW-HA Treatment

Spot no.	Swiss-prot no.	Protein name	MW	pI	No. matched peptides	MOWSE score	Seq cov. (%)	Subcellular location	Functional classification	0.05% HMW-HA/ UVB treated[a]	0.3% HMW-HA/ UVB treated[a]	0.3% HMW-HA/0.05% HMW-HA[a]	Representative matched peptides
507	P13645	Keratin, type I cytoskeletal 10[c]	59,703	5.13	7	65/56	11	Cytoplasm	Cytoskeleton	1.35	2.3	1.7	K.GSLGGGFSSGGFSGGSFSR.GK. HGNSHQGEPR.D
550	O43852	Calumenin[c]	37,198	4.47	6	82/56	26	Endoplasmic Reticulum	Signal transduction/ Ca regulation	1.27	1.49	1.17	K.VHNDAQSFDYDHDAFLGAEEAK. TK.TFDQLTPEESKER.L
1145	O75347	Tubulin-specific chaperone A[c]	12,904	5.25	7	60/56	37	Cytoplasm	Protein folding	1.3	1.46	1.12	K.QAEILQESR.MR.RLEAAYLDLQR.I
275	P13645	Keratin, type I cytoskeletal 10[c]	59,703	5.13	6	65/56	8	Cytoplasm	Cytoskeleton	1.2	1.39	1.16	K.GSLGGGFSSGGFSGGSFSR.GR. LKYENEVALR.Q
549	P05783	Keratin, type I cytoskeletal 18[c]	48,029	5.34	12	114/56	20	Cytoplasm	Cytoskeleton	1.09	1.38	1.27	R.STFSTNYR.SR.LASYLDR.V
704	Q9Y2Z0	Suppressor of G2 allele of SKP1 homolog[c]	41,284	5.07	5	58/56	15	Cytoplasm	Protein degradation	1.43	1.33	−1.07	K.ALEQKPDDAQYYCQR.AK.LDIETGFHR.V
250	P27797	Calreticulin[b]	48,283	4.29	1	115/56 (MS/MS)	2	Endoplasmic Reticulum	Signal transduction/ Ca regulation	1.39	1.3	−1.07	K.EQFLDGDGWTSR.W
429	P05787	Keratin, type II cytoskeletal 8[b]	53,671	5.52	9	83/56	21	Cytoplasm	Cytoskeleton	1.34	1.3	−1.03	K.WSLLQQQKTAR.SR.LEGLTDEINFLR.Q
809	P21796	Voltage-dependent anion-selective channel protein 1[c]	30,868	8.62	6	76/56	26	Mitochondrion	Transport	1.4	1.29	−1.08	K.GYGFGLIK.LR.WTEYGLTFTEK.W
706	P04075	Fructose-bisphosphate aldolase A[c]	39,851	8.3	6	77/56	28	Cytoplasm	Metabolism	1.36	1.26	−1.09	M.PYQYPALTPEQK.KK.ADDGRPFPQVIK.S
993	P09211	Glutathione S-transferase P[b]	23,569	5.43	7	102/56	45	Cytoplasm	Redox regulation	1.37	1.26	−1.09	M.PPYTVVYFPVR.GK. FQDGDLTLYQSNTILR.H
525	P05783	Keratin, type I cytoskeletal 18[c]	48,029	5.34	7	68/56	14	Cytoplasm	Cytoskeleton	−1.47	1.24	1.82	R.STFSTNYR.SR.DWSHYFK.I
180	P38646	Stress-70 protein, mitochondrial[c]	73,920	5.87	9	93/56	16	Mitochondrion	Protein folding	1.41	1.24	−1.14	R.TTPSVVAFTADGER.LK. NAVITVPAYFNDSQR.Q
964	P60174	Triosephosphate isomerase[b]	26,938	6.45	7	103/56	39	Cytoplasm	Carbohydrate metabolism	1.37	1.16	−1.19	K.FFVGGNWK.MK. VPADTEVVCAPPTAYIDFAR.Q
195	P08107	Heat shock 70 kDa protein 1[b]	70,294	5.48	6	66/56	11	Cytoplasm	Protein folding	1.61	1.14	−1.41	R.TTPSYVAFTDTER.LK. DAGVIAGLNVLR.I
966	P60174	Triosephosphate isomerase[b,d]	26,938	6.45	3	91/56 98/56 (MS/MS) 79/56 (MS/MS)	325	Cytoplasm	Carbohydrate metabolism	1.38	1.13	−1.22	R.KFFVGGNWK.MK. VPADTEVVCAPPTAYIDFAR.Q
700	P04264	Keratin, type II cytoskeletal 1[c]	66,149	8.16	6	66/56	15	Cell Membrane	Cytoskeleton	1.3	1.12	−1.16	R.SGGGFSSGSAGIINYQR.R R.FLEQQNQVLQTK.W
154	P11021	78 kDa glucose-regulated protein[b]	72,402	5.07	14	138/56	22	Endoplasmic Reticulum	Biosynthesis	1.3	1.04	−1.25	R.VEIIANDQGNR.IR.ITPSYVAFTPEGER.L
477	Q8WUD1	Ras-related protein Rab-2B[c]	24,427	7.68	5	72/56	24	Cell Membrane	Signal transduction	1.32	1.03	−1.29	R.SITRSYYR.GR.GAAGALLVYDITRR.E

[a]Average ratio of differential expression ($P < 0.05$) of UVB-irradiated HCE-2 cells in response to 0.3% HMW-HA/0.05% HMW-HA treatments with a great than 1.3-fold differences are listed in this table.
[b]Identified proteins are common to treatments with UVB and UVB + HA.
[c]Identified proteins are specific for HA treatment but not for UVB treatment.
[d]These proteins have been identified by MALDI-TOF/TOF MS. The parameters (sequence coverages, MASCOT values, matched peptide numbers, and matched peptide sequences) are obtained from MALDI-TOF/TOF MS sequence analysis.

TABLE IV. Alphabetic List of Identified Differentially Down-Regulated Proteins After 2D-DIGE Coupled With MALDI-TOF Mass Spectrometry Analysis in UVB-Irradiated HCE-2 Cells in Response to HMW-HA Treatment

Spot no.	Swiss-prot no.	Protein name	MW	pI	No. matched peptides	MOWSE score	Seq cov. (%)	Subcellular location	Functional classification	0.05% HMW-HA/UVB treated[a]	0.3% HMW-HA/UVB treated[a]	0.3% HMW-HA/0.05% HMW-HA[a]	Representative matched peptides
912	P63104	14-3-3 protein zeta/delta[c]	27,8994.73		9	98/56	35	Cytoplasm	Signal transduction	−1.3	−1.21	1.08	K.NELVQKAK.LK.SVTEQGAELSNEER.N
523	P60709	Actin, cytoplasmic 1[c]	42,0525.29		8	77/56	26	Cytoplasm	Cytoskeleton	−1.71	−1.01	1.69	K.AGFAGDDAPR.AK.IWHHTFYNELR.V
558	P60709	Actin, cytoplasmic 1[c]	42,0525.29		7	76/56	26	Cytoplasm	Cytoskeleton	−1.45	−1.08	1.34	K.AGFAGDDAPR.AK.IWHHTFYNELR.V
1265	P54819	Adenylate kinase isoenzyme 2, mitochondrial[b]	26,6897.67		1	57/56 (MS/MS)	4	Mitochondrion	Biosynthesis	−1.36	−1.22	1.12	K.NGFLLDGFPR.T
508	P31930	Cytochrome b-c1 complex subunit 1, mitochondrial[c]	53,2975.94		7	67/56	15	Mitochondrion	Electron transport	−2.63	−1.99	1.32	K.NNGAGYFLEHLAFK.G R. NALVSHLDGTTPVCEDIGR.S
536	Q8N3Y1	F-box/WD repeat-containing protein 8[c]	67,7685.32		5	66/56	11	Cytoplasm	Protein degradation	−1.33	−1.06	1.26	R.ARRPEVGSGR.SR.AEGQDVASRSR.S
779	P04406	Glyceraldehyde-3-phosphate dehydrogenase[c]	36,2018.57		5	69/56	17	Cytoplasm	Carbohydrate metabolism	1.17	−1.33	−1.56	K.VGVNGFGR.IK.LVINGNPITIFQER.D
867	P63244	Guanine nucleotide-binding protein subunit beta-2-like 1[b]	35,511	7.6	7	104/56	28	Cell Membrane	Signal transduction	−1.32	−1.17	1.13	R.DETNYGIPQR.AR.LWDLTTGTTTR.R
1102	P19105	Myosin regulatory light chain MRLC3[b]	19,8394.67		8	97/56	57	Cytoplasm	Cell motility	−1.12	−1.46	−1.3	K.LNGTDPEDVIR.NR. NAFACFDEEATGTIQEDYLR.E
828	P48739	Phosphatidylinositol transfer protein beta isoform[c]	31,8056.41		6	81/56	18	Cytoplasm	Transport	−1.25	−1.49	−1.2	K.SKVPAFVR.MK.AWNAYPYCR.T
362	P68363	Tubulin alpha-1B chain[b]	50,8044.94		9	120/56	26	Cytoplasm	Cytoskeleton	−3.14	−2.14	1.47	R.AVFVDLEPTVIDEVR.TR. QLFHPEQLITGK.E
1275	P07437	Tubulin beta chain[b]	50,0954.78		7	76/56	19	Cytoplasm	Cytoskeleton	−1.41	−1.17	1.2	R.AILVDLEPGTMDSVR.SK. GHYTEGAELVDSVLDVVR.K
1067	O75223	Uncharacterized protein C7orf24/Gamma-glutamylcyclotransferase[c,d]	21,2225.07		1	114/56 (MS/MS)	5	Cytoplasm	Redox regulation	−1.37	−1.11	1.23	R.NPSAAFFCVAR.L

[a]Average ratio of differential expression ($P < 0.05$) of UVB-irradiated HCE-2 cells in response to 0.3% HMW-HA/0.05% HMW-HA treatments with a less than −1.3-fold differences are listed in this table.
[b]Identified proteins are common to treatments with UVB and UVB + HA.
[c]Identified proteins are specific for HA treatment but not for UVB treatment.
[d]These proteins have been identified by MALDI-TOF/TOF MS. The parameters (sequence coverages, MASCOT values, matched peptide numbers, and matched peptide sequences) are obtained from MALDI-TOF/TOF MS sequence analysis.

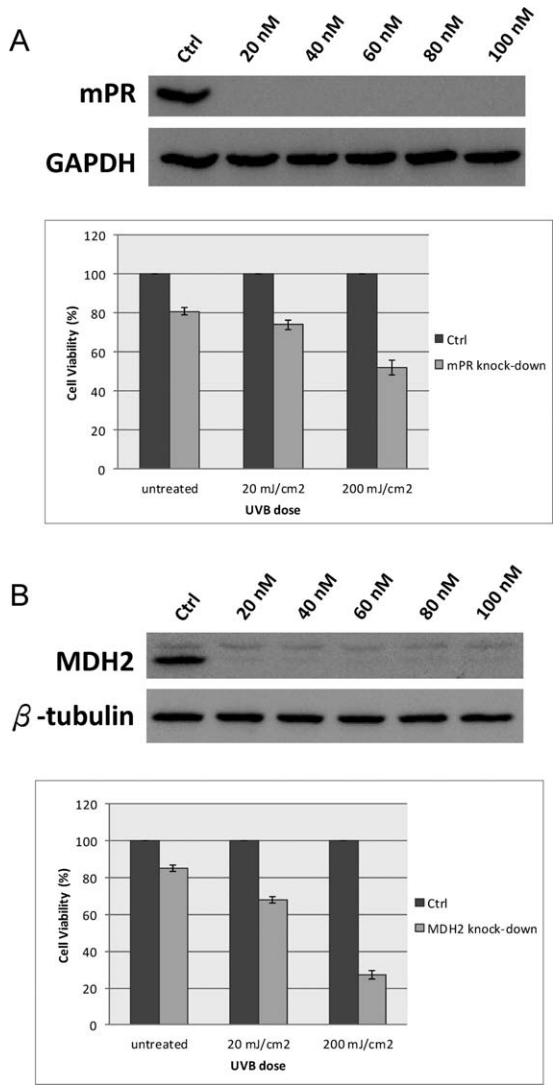

Fig. 10. Effect of UVB-irradiation on cell proliferation of mPR siRNA and MDH2 siRNA-silenced HCE-2 cells. Efficiency of mPR siRNA and MDH2 siRNA on the inhibition of mPR and MDH2 expression in HCE-2 cells were determined with siRNA silencing and immunoblot analysis. HCE-2 cells grown overnight were treated with indicated concentrations of mPR-specific siRNA (**A**) or 60 nM MDH2-specific siRNA (**B**) for 24 hr. Expression of mPR and MDH2 in HCE-2 cells were monitored with immunoblotting by using primary antibodies against mPR and MDH2, respectively. MTT-based proliferation assays were subsequently performed where 5,000 HCE-2 cells seeded into 96-well plate for overnight incubation followed by pre-treated with (A) 60 nM mPR-specific siRNA or (B) 60 nM MDH2-specific siRNA combining with corresponding scramble siRNA. After 24 hr, cells were irradiated with indicated doses of UVB followed by incubated with MTT and then DMSO added and the plates shaken for 20 min followed by measurement of the absorbance at 540 nm. Values were normalized against the scramble siRNA samples and are the average of six independent measurements ± SD.

data are associated with protein deregulation including calpain, cofilin-1, fascin, LIM, SH3 domain protein 1, microtubule-associated protein RP/EB family member 1, profilin-1, and tubulins in our proteomic analysis. The in vitro incubation with HA significantly reversed certain UVB-induced corneal epithelial cell responses. HA, a viscous biopolymer covered on the outer surface of the plasma membrane, has been reported to potentially neutralize ROS and cytotoxins [Nakamura et al., 1997; Pauloin et al., 2009; Yang et al., 2010]. A previous report indicated that actinoquinol-HA eye drops reduced alterations in the corneal optics and suppressed oxidative damage in UVB-irradiated corneas. However, the effective corneal protection provided by these eye drops was limited to the lower UVB dose [Cejka et al., 2010]. The biological functions of HA rely on its number of disaccharides [Toole, 2004a]. Accordingly, we focused on the correlation between the molecular weight of HA and its ability against UVB-induced corneal epithelial cell damage. We initially aimed to clarify the role of HA during UVB irradiation. The results showed that HMW-HA was superior to LMW-HA in reducing the toxic UVB-induced effects and recovering UVB-induced impairments in wound healing and cell migration. HMW-HA was also found to modulate the expression of cytoskeletal proteins (such as actins and tubulins) and migration-regulated proteins (such as myosin regulatory light chain MRLC3) after encountering UVB-induced damage. Our immunofluorescence data also suggested that HMW-HA might promote F-actin polarity and restore the wound closure ability implying HMW-HA, presumably leading to the efficient regulation of protrusion dynamics and the wound healing of UVB-damaged corneal cells.

HA was reported to specifically act with cell-surface receptor protein CD44 [Toole, 2004]. The interaction between CD44 and HA is recognized as important in wound healing and tumor metastasis [Isacke and Yarwood, 2002]. A previous report demonstrated that CD44 activation increases the secretion of matrix metalloproteinase-2 (MMP-2) to stimulate cell migration, wound healing, and cancer cell metastasis through the aid of matrix metalloproteinase-14 (MMP-14) [Takahashi et al., 1999]. A recent report showed that HMW-HA stimulates cell differentiation but has no considerable effect on the CD44 level, whereas LMW-HA inhibits cell differentiation and diminishes the CD44 level. This finding suggests that HMW-HA is more potent in wound healing compared to the wound-healing ability of LMW-HA because of the differential expression of CD44 [Maharjan et al., 2011]. Our data are in agreement with these observations, demonstrating that HMW-HA has a significant effect on UVB-induced corneal epithelial wound healing. The CD44 receptor has also been shown to express on the surface of corneal epithelial cells [Pauloin et al., 2008], implying a close relationship between HA and the plasma membrane through the CD44 receptor in maintaining the plasma membrane integrity of corneal cells during UVB-induced damage. Apart from the molecular weight, our

findings showed that the HA concentration is crucial for protecting corneal cells from UVB-induced injury. Our data showed that 0.3% HMW-HA is the optimal concentration for protecting corneal epithelial cells from UVB-induced damage. At this concentration, HMW-HA might constitute a proper biopolymer structure that covers the outer surface of the plasma membrane by interacting with the CD44 receptors. The CD44-bound HMW-HA might thus promote cell proliferation signals [Wang et al., 2011] or mask death receptors from activation to maintain cell function and survival [Pauloin et al., 2009]. Cell proliferation and protection ability dropped dramatically if the HMW-HA concentration was higher than 0.5% (data not shown), implying that high concentrations of HA might interrupt the metabolism, nutrients, and gas exchange. Miyauchi et al. [1990] reported a similar observation, showing that concentrated HA is substantially more viscous than the culture medium that inhibits epithelial migration, nutrient diffusion, and cell metabolism.

In our proteomic analysis of UVB-irradiated corneal cells, we selected 2 potential target proteins, mPR and MDH2, for further evaluation of their roles in the response to UVB irradiation because they each exhibited significant upregulation in UVB-irradiated HCE-2 during proteomic analysis and were shown to play roles in cell signaling and exchanging reduced equivalents. Previous studies have shown that cancer cells overexpress mPR compared to normal cells, and thus, mPR is recognized as an important marker for tumors and cancer progression [Cahill, 2007; Xu et al., 2011]. The mPR protein is involved in the control of cancer cell proliferation and growth [Neubauer et al., 2009] through direct interactions between its cytochrome b5-binding domain and target proteins, such as Insig-1 [Yang et al., 2002]. Recent studies have reported that mPR mediates the progesterone anti-apoptotic function [Peluso et al., 2006] and induces Akt phosphorylation to promote cell survival [Neubauer et al., 2008]. However, no study has reported the role of mPR in the cell response to UVB. Thus, our result suggests that mPR might protect corneal cells from UVB-induced damage through the activation of the PI3 kinase pathway. The second target protein, MDH2, catalyzes malate oxidation in the TCA cycle and generates NADPH in the malate-aspartate shuttle. The generated NADPH is an important source for the reducing power of cells, which might reduce UVB-induced ROS in corneal cells.

A recent study reported that ERp29 overexpression attenuates cell apoptosis through the upregulation of heat shock protein beta-1 in breast cancer cells [Zhang and Putti, 2010]. This observation is in partial agreement with our study, which shows that both ERp29 and heat shock protein beta-1 exhibit significant upregulation in expression following the UVB irradiation of HCE-2 cells. The ERp29 protein may downregulate eIF2α expression and further stimulates the activity of heat shock protein beta-1. This process might alleviate unfolded and misfolded protein-induced ER stress in UVB-irradiated HCE-2 cells.

During UVB irradiation, numerous ROS accumulate, leading to cell damage or even cell death. Cells accordingly develop defense mechanisms, including the overexpression of redox-modulated proteins to scavenge UVB-induced ROS. We demonstrated the upregulation of glutathione *S*-transferase P, peroxiredoxin-1, peroxiredoxin-4, Protein DJ-1, and thioredoxin-dependent peroxide reductase in UVB-irradiated HCE-2 cells, implying that these redox-regulatory proteins reduce ROS levels and prevent ROS-induced cytotoxicity in UVB-irradiated cells. A similar report by Black et al. revealed that UVB modulates the corneal epithelial cell expression of antioxidants (Mn-SOD, catalase, heme oxygenase-1, and glutathione *S*-transferase) and proinflammatory mediators (interferon-gamma, IL-1beta, TGF-beta, TNF-alpha, and cyclooxygenase-2). Alterations in the expression of these mediators are likely important in regulating inflammation and protecting the cornea from UVB-induced oxidative stress [Black et al., 2011].

Several key regulatory proteins mediate the interaction of heat shock proteins to inhibit apoptosis. The intrinsic pathway of caspase-mediated apoptosis is stimulated by c-Jun kinase, resulting in the release of cytochrome c from the mitochondria, and the subsequent activation of a caspase cascade involving caspase 8 and caspase 3. They are each inhibited by heat shock cognate 71, which interacts with Bcl-2 through Bag-1, enabling incorporation of the complex into the mitochondrial membrane to inhibit apoptosis [Takayama et al., 1998]. Heat shock protein beta-1 inhibits the extrinsic apoptotic pathway of caspase 9 through death receptors [Concannon et al., 2001; Hsu et al., 2011]. In this study, heat shock cognate 71 and heat shock protein beta-1 were both upregulated in UVB-irradiated HCE-2 cells, implying that heat shock cognate 71 and heat shock protein beta-1 are essential for protecting HCE-2 cells from UVB-induced apoptosis.

In conclusion, we performed a comprehensive proteomic analysis after irradiating corneal epithelial cells with UVB. We identified differentially expressed proteins participating in numerous cellular responses against UVB irradiation. We also showed that HMW-HA significantly reduces UVB-induced cytotoxic effects in corneal cells and increases cell migration and the wound-healing ability. We confirmed the potency of mPR and MDH2 in protecting corneal cells from UVB irradiation. Thus, our study serves as a suitable reference for clinical practice. Our findings can be applied to eye drops in repairing UVB-induced damage of the ocular surface and may be used to design biomaterials to accelerate wound healing.

AUTHOR CONTRIBUTIONS

Dr HL Chan designed the study and prepared the manuscript draft. JM Li and CL Wu performed the experiments. Dr HC Chou performed data analysis and prepared draft figures and tables. All authors approved the final manuscript.

REFERENCES

Ardan T, Cejkova J. 2012. Immunohistochemical expression of matrix metalloproteinases in the rabbit corneal epithelium upon UVA and UVB irradiation. Acta Histochem 114:540-546.

Black AT, Gordon MK, Heck DE, Gallo MA, Laskin DL, Laskin JD. 2011a. UVB light regulates expression of antioxidants and inflammatory mediators in human corneal epithelial cells. Biochem Pharmacol 81:873-880.

Cahill MA. 2007. Progesterone receptor membrane component 1: An integrative review. J Steroid Biochem Mol Biol 105:16-36.

Cejka C, Luyckx J, Ardan T, Platenik J, Sirc J, Michalek J, Cejkova J. 2010. The effect of actinoquinol with hyaluronic acid in eye drops on the optical properties and oxidative damage of the rabbit cornea irradiated with UVB rays. Photochem Photobiol 86: 1294-1306.

Cejkova J, Ardan T, Cejka C, Kovaceva J, Zidek Z. 2005. Irradiation of the rabbit cornea with UVB rays stimulates the expression of nitric oxide synthases-generated nitric oxide and the formation of cytotoxic nitrogen-related oxidants. Histol Histopathol 20:467-473.

Cejkova J, Stipek S, Crkovska J, Ardan T. 2000. Changes of superoxide dismutase, catalase and glutathione peroxidase in the corneal epithelium after UVB rays. Histochemical and biochemical study. Histol Histopathol 15:1043-1050.

Chan HL, Gaffney PR, Waterfield MD, Anderle H, Peter MH, Schwarz HP, Turecek PL, Timms JF. 2006. Proteomic analysis of UVC irradiation-induced damage of plasma proteins: serum amyloid P component as a major target of photolysis. FEBS Lett 580:3229-3236.

Chan HL, Gharbi S, Gaffney PR, Cramer R, Waterfield MD, Timms JF. 2005. Proteomic analysis of redox- and Erbb2-dependent changes in mammary luminal epithelial cells using cysteine- and lysine-labelling two-dimensional difference gel electrophoresis. Proteomics 5:2908-2926.

Chen YW, Chou HC, Lyu PC, Yin HS, Huang FL, Chang WS, Fan CY, Tu IF, Lai TC, Lin ST, Lu YC, Wu CL, Huang SH, Chan HL. 2011a. Mitochondrial proteomics analysis of tumorigenic and metastatic breast cancer markers. Funct Integr Genomics 11:225-239.

Chen YW, Liu JY, Lin ST, Li JM, Huang SH, Chen JY, Wu JY, Kuo CC, Wu CL, Lu YC, Chen YH, Fan CY, Huang PC, Law CH, Lyu PC, Chou HC, Chan HL. 2011b. Proteomic analysis of gemcitabine-induced drug resistance in pancreatic cancer cells. Mol Biosyst 7:3065-3074.

Chou HC, Chen YW, Lee TR, Wu FS, Chan HT, Lyu PC, Timms JF, Chan HL. 2010. Proteomics study of oxidative stress and Src kinase inhibition in H9C2 cardiomyocytes: A cell model of heart ischemia reperfusion injury and treatment. Free Radic Biol Med 49:96-108.

Chou HC, Lu YC, Cheng CS, Chen YW, Lyu PC, Lin CW, Timms JF, Chan HL. 2012. Proteomic and redox-proteomic analysis of berberine-induced cytotoxicity in breast cancer cells. J. Proteomics 75:3158-3176.

Chung JH, Kim HJ, Fagerholmb P, Cho BC. 1996. Effect of topically applied Na-hyaluronan on experimental corneal alkali wound healing. Korean J Ophthalmol 10:68-75.

Concannon CG, Orrenius S, Samali A. 2001. Hsp27 inhibits cytochrome C-mediated caspase activation by sequestering both pro-caspase-3 and cytochrome C. Gene Expr 9:195-201.

Downes JE, Swann PG, Holmes RS. 1994. Differential corneal sensitivity to ultraviolet light among inbred strains of mice. Correlation of ultraviolet B sensitivity with aldehyde dehydrogenase deficiency. Cornea 13:67-72.

Fitzsimmons TD, Molander N, Stenevi U, Fagerholm P, Schenholm M, Von Malmborg A. 1994. Endogenous hyaluronan in corneal disease. Invest Ophthalmol Vis Sci 35:2774-2782.

Hsu HS, Lin JH, Huang WC, Hsu TW, Su K, Chiou SH, Tsai YT, Hung SC. 2011. Chemoresistance of lung cancer stemlike cells depends on activation of Hsp27. Cancer 117:1516-1528.

Huang HL, Hsing HW, Lai TC, Chen YW, Lee TR, Chan HT, Lyu PC, Wu CL, Lu YC, Lin ST, Lin CW, Lai CH, Chang HT, Chou HC, Chan HL. 2010. Trypsin-induced proteome alteration during cell subculture in mammalian cells. J Biomed Sci 17:36.

Hung PH, Chen YW, Cheng KC, Chou HC, Lyu PC, Lu YC, Lee YR, Wu CT, Chan HL. 2011. Plasma proteomic analysis of the critical limb ischemia markers in diabetic patients with hemodialysis. Mol Biosyst 7:1990-1998.

Isacke CM, Yarwood H. 2002. The hyaluronan receptor, CD44. Int J Biochem Cell Biol 34:718-721.

Kolozsvari L, Nogradi A, Hopp B, Bor Z. 2002. UV absorbance of the human cornea in the 240- To 400-Nm range. Invest Ophthalmol Vis Sci 43:2165-2168.

Lai TC, Chou HC, Chen YW, Lee TR, Chan HT, Shen HH, Lee WT, Lin ST, Lu YC, Wu CL, Chan HL. 2010. Secretomic and proteomic analysis of potential breast cancer markers by two-dimensional differential gel electrophoresis. J. Proteome Res 9:1302-1322.

Lin CP, Chen YW, Liu WH, Chou HC, Chang YP, Lin ST, Li JM, Jian SF, Lee YR, Chan HL. 2011. Proteomic identification of plasma biomarkers in uterine leiomyoma. Mol. Biosyst 8:1136-1145.

Lodovici M, Raimondi L, Guglielmi F, Gemignani S, Dolara P. 2003a. Protection against ultraviolet B-induced oxidative DNA damage in rabbit corneal-derived cells (SIRC) by 4-coumaric acid. Toxicology 184:141-147.

Maharjan AS, Pilling D, Gomer RH. 2011. High and low molecular weight hyaluronic acid differentially regulate human fibrocyte differentiation. PLoS One 6:E26078.

Miyauchi S, Sugiyama T, Machida A, Sekiguchi T, Miyazaki K, Tokuyasu K, Nakazawa K. 1990. The effect of sodium hyaluronate on the migration of rabbit corneal epithelium. I. An in vitro study. J Ocul Pharmacol 6:91-99.

Nakamura M, Sato N, Chikama TI, Hasegawa Y, Nishida T. 1997. Hyaluronan facilitates corneal epithelial wound healing in diabetic rats. Exp Eye Res 64:1043-1050.

Neubauer H, Adam G, Seeger H, Mueck AO, Solomayer E, Wallwiener D, Cahill MA, Fehm T. 2009. Membrane-initiated effects of progesterone on proliferation and activation of VEGF in breast cancer cells. Climacteric 12:230-239.

Neubauer H, Clare SE, Wozny W, Schwall GP, Poznanovic S, Stegmann W, Vogel U, Sotlar K, Wallwiener D, Kurek R, Fehm T, Cahill MA. 2008. Breast cancer proteomics reveals correlation between estrogen receptor status and differential phosphorylation of PGRMC1. Breast Cancer Res 10:R85.

Okada H, Mak TW. 2004. Pathways of apoptotic and non-apoptotic death in tumour cells. Nat Rev Cancer 4:592-603.

Pauloin T, Dutot M, Joly F, Warnet JM, Rat P. 2009b. High molecular weight hyaluronan decreases uvb-induced apoptosis and inflammation in human epithelial corneal cells. Mol Vis 15:577-583.

Pauloin T, Dutot M, Liang H, Chavinier E, Warnet JM, Rat P. 2009c. Corneal protection with high-molecular-weight hyaluronan against in vitro and in vivo sodium lauryl sulfate-induced toxic effects. Cornea 28:1032-1041.

Pauloin T, Dutot M, Warnet JM, Rat P. 2008. In vitro modulation of preservative toxicity: High molecular weight hyaluronan decreases apoptosis and oxidative stress induced by benzalkonium Chloride. Eur J Pharm Sci 34:263-273.

Peluso JJ, Pappalardo A, Losel R, Wehling M. 2006. Progesterone membrane receptor component 1 Expression In The Immature Rat Ovary And Its Role In Mediating Progesterone's Antiapoptotic Action. Endocrinology 147:3133-3140.

Shi B, Han B, Schwab IR, Isseroff RR. 2006. UVB irradiation-induced changes in the 27-Kd heat shock protein (HSP27) in human corneal epithelial cells. Cornea 25:948-955.

Takahashi K, Eto H, Tanabe KK. 1999. Involvement of CD44 in matrix metalloproteinase-2 regulation in human melanoma cells. Int J Cancer 80:387-395.

Takayama S, Krajewski S, Krajewska M, Kitada S, Zapata JM, Kochel K, Knee D, Scudiero D, Tudor G, Miller GJ, Miyashita T, Yamada M, Reed JC. 1998. Expression and location of Hsp70/Hsc-binding anti-apoptotic protein BAG-1 and its variants in normal tissues and tumor cell lines. Cancer Res 58:3116-3131.

Toole BP. 2004a. Hyaluronan: From extracellular glue to pericellular cue. Nat Rev Cancer 4:528-539.

Wang YZ, Cao ML, Liu YW, He YQ, Yang CX, Gao F. 2011. CD44 mediates oligosaccharides of hyaluronan-induced proliferation, #tube formation and signal transduction in endothelial cells. Exp Biol Med (Maywood) 236:84-90.

Wu CL, Chou HC, Cheng CS, Li JM, Lin ST, Chen YW, Chan HL. 2012. Proteomic analysis of uvb-induced protein expression- and redox-dependent changes in skin fibroblasts using lysine- and cysteine-labeling two-dimensional difference gel electrophoresis. J Proteomics 75:1991-2014.

Xu J, Zeng C, Chu W, Pan F, Rothfuss JM, Zhang F, Tu Z, Zhou D, Zeng D, Vangveravong S, Johnston F, Spitzer D, Chang KC, Hotchkiss RS, Hawkins WG, Wheeler KT, Mach RH. 2011. Identification of the PGRMC1 protein complex as the putative sigma-2 receptor binding site. Nat Commun 2:380.

Yang G, Espandar L, Mamalis N, Prestwich GD 2010. A cross-linked hyaluronan gel accelerates healing of corneal epithelial abrasion and alkali burn injuries in rabbits. Vet Ophthalmol 13:144-150.

Yang T, Espenshade PJ, Wright ME, Yabe D, Gong Y, Aebersold R, Goldstein JL, Brown MS. 2002. Crucial step in cholesterol homeostasis: Sterols promote binding of SCAP to INSIG-1, a membrane protein that facilitates retention of Srebps in ER. Cell 110: 489-500.

Zhang D, Putti TC. 2010. Over-expression of Erp29 attenuates doxorubicin-induced cell apoptosis through up-regulation of Hsp27 in breast cancer cells. Exp Cell Res 316:3522-3531.

Accepted by—
C. Menck